## General Disclaimer

### One or more of the Following Statements may affect this Document

- This document has been reproduced from the best copy furnished by the organizational source. It is being released in the interest of making available as much information as possible.

- This document may contain data, which exceeds the sheet parameters. It was furnished in this condition by the organizational source and is the best copy available.

- This document may contain tone-on-tone or color graphs, charts and/or pictures, which have been reproduced in black and white.

- This document is paginated as submitted by the original source.

- Portions of this document are not fully legible due to the historical nature of some of the material. However, it is the best reproduction available from the original submission.

NASA Contractor Report 168279


# EXPERIMENTAL STUDY OF THE OPERATING CHARACTERISTICS OF PREMIXING-PREVAPORIZING FUEL/AIR MIXING PASSAGES

David A. Rohy and J. G. Meier

Solar Turbines Incorporated
San Diego, California



November 1983

Prepared for

NATIONAL AERONAUTICS AND SPACE ADMINISTRATION
Lewis Research Center
Under Contract NAS3-20662

# TABLE OF CONTENTS

## GLOSSARY

NASA - National Aeronautics and Space Administration
ALEC - Advanced Low Emission Combustor
LPP - Lean Premixed, Prevaporized
LDV - Laser Doppler Velocimeter
SDL - Spectron Development Laboratories

# 1

# INTRODUCTION

The program described in this report had as a goal the characterization of fuel sprays to be utilized in calibrating and verifying an analytical model of a premixing-prevaporizing passage of a lean burning combustor.

NASA's Advanced Low Emission Combustor Program (ALEC) was initiated to apply modern techniques of combustion science and analysis to the problems of achieving significant reductions in gas turbine pollutant emissions while maintaining high performance and durability for a wide range of aviation fuels. From this program, the lean premixed-prevaporized (LPP) combustor has evolved as the primary candidate for the program goals.

The LPP combustor is similar to conventional combustor concepts except that, prior to combustion, the fuel and air are mixed and the fuel vaporized in a fuel preparation section; hence the term premixed and prevaporized. This premixing and pevaporization is necessary to achieve the uniformity and control over local stoichiometry for low pollutant emissions, and low levels of flame radiation and pattern factors conducive to improved durability and performance for a variety of fuels.

In order to assist the design of the LPP combustor and reduce the associated development risks, an analytical model of the fuel preparation process is desirable. Such a model would permit low cost computer screening of premixing passage concepts and reduce time consuming, expensive experimental evaluation of high potential candiates. Such a model is currently being developed. The model computes the fuel-air distribution, degree of fuel vaporization, residual dropsize, distribution and air velocity, pressure and temperature profiles at the exit of the fuel preparation section, given the inlet air flow conditions and fuel spray characteristics.

Under the present program, data was collected on fuel spray and air flow characteristics at several points within a fuel preparation duct to calibrate and verify this analytical model. A well controlled test rig capable of producing repeatable fuel sprays was utilized in the research program. The rig was designed to operate to pressures of 10 atmospheres and to inlet temperatures of 750K.
The use of advanced non-intrusive (optical) measurement techniques for fuel spray characterization is seen as a significant contribution of this program. The data set obtained is the first acquired by this method at high pressures and temperature and is significantly more detailed than any previously obtained.

# 2

# EXPERIMENTAL DESIGN

## 2.1 DESIGN PHILOSOPHY

Combustion research, relating to the operational characteristics of both innovative systems and the more well-established devices such as gas turbine combustors, requires instrumentation which can provide measurements in extremely severe environments. In an environment where pressures may reach 600 psi and temperatures over a thousand degrees Celcius, mechanical devices such as hot wire anemometers designed to function in much less severe conditions quickly fail or become highly inaccurate. Furthermore, instrumentation requiring a mechanical sampling technique perturb the environment which is to be measured. This perturbation reduces their accuracy and reliability. One particular area where instrumentation needs have become critical is in the measurement of particle (droplet) size and velocity for fuel sprays during fuel/air preparation and combustion. Devices which utilize optical measurements of the desired parameters are non-intrusive and thus can operate in severe environments with no perturbation of the flow field.

An instrument which has undergone extensive development during the past ten years, and has shown its utility in a wide variety of applications, is the Laser Doppler Velocimeter (LDV). Using a laser as a coherent light source, this instrument has been used to measure particle velocities in fluids. These applications have ranged from low speed water flows through supersonic wind tunnels to large oil and gas flames. The velocity measurement is obtained by determining the Doppler shift of light scattered from particles passing through the laser beam. This program has used a well-developed version of one type of Laser Doppler Velocimeter (LDV) optical system which incorporated highly refined signal analysis and electronic instrumentation to determine not only particle velocity but also particle size. This system has been tested with excellent results in small wind tunnels for the measurement of droplets in water sprays.

The primary use of the LDV instrumentation is to characterize the spray from various fuel injectors at several sets of operating conditions. The spray is characterized by measuring the droplet size and velocity at a set of points in several planes downstream of the injector. In order to achieve data that is meaningful, the test conditions (air flow, temperature, pressure, etc.) must remain constant during the measurement period and be repeatable from one test session to the next. This type of stability is especially important when comparing spray distributions from different injectors. The rig must also provide access for complete instrumentaton to allow for flow measurement. The completed rig, as described below, allows for repeatability and stability. In addition, it has provision for instrumentation and fuel burnoff.

## 2.2 RIG DESIGN

The "rig" includes the fuel/air preparation section, burnoff combustor, air pressure regulation valve and supporting subassemblies. Basically the constraints were:

- The air inlet preparation section has been designed to produce uniform flat profiles of total pressure, total temperature and velocity at the inlet plane to the fuel injection section.

- The fuel injection section and fuel/air mixing section have a rectangular cross section with inside dimensions of 7.62 cm by 7.62 cm.

- The fuel injection section is designed to produce uniform flat profiles of total pressure, total temperature and velocity immediately upstream of the fuel injector location. It is also designed to accommodate various types of fuel injectors. (The injectors are mounted on a spool piece (2.5 cm high) and inserted into the flow path.)

- The fuel/air mixing section is designed to avoid autoignition and flashback over the conditions of the tests. It was designed to allow for optical measurements 7.5 cm, 15 cm, and 30 cm downstream of the fuel injector. This was accomplished with a stationary window and the addition of blank spool pieces to move the injector and fuel/air mixing section further upstream of the window. The spools were 7.5 cm, 15 cm and 30 cm high.

- The rig is designed to operate at temperatures of 450 to 750K, 20.0 to 80.0 m/sec reference velocity, equivalence ratios of 0.3 to 0.5 and pressures up to 10 atm.

- Flow distortions due to ports and instrumentation were minimized.

The rig was assembled in a manner shown in Figures 1 and 2. An A-frame support is used to support the rig vertically so that gravity will not disturb the radial symmetry of the spray distribution. The major components and dimensions of the rig are called out in the sketch of the rig in Figure 3.

The liquid fuel injector flange assembly is shown in Figure 4 and 5. It was designed to allow for changes in the type of injector under study. The fuel enters the air strut from both sides to prevent coking. Instrumentation ports were installed 180 degrees opposed. The injector for the first test has an ID = 0.085 cm and protrudes about 0.64 cm from the strut. This design produced a narrow spray cone and a distribution of fine droplets. Others designs without the sharp edge around the injector produced larger droplets and a less uniform combustion in the afterburner. (Standard gas turbine injectors cannot be used on the rig because the spray angle is generally too wide. They would have deposited fuel on the wall within centimeters of the injector.) All optical measurements were made with the injector shown in Figure 5.

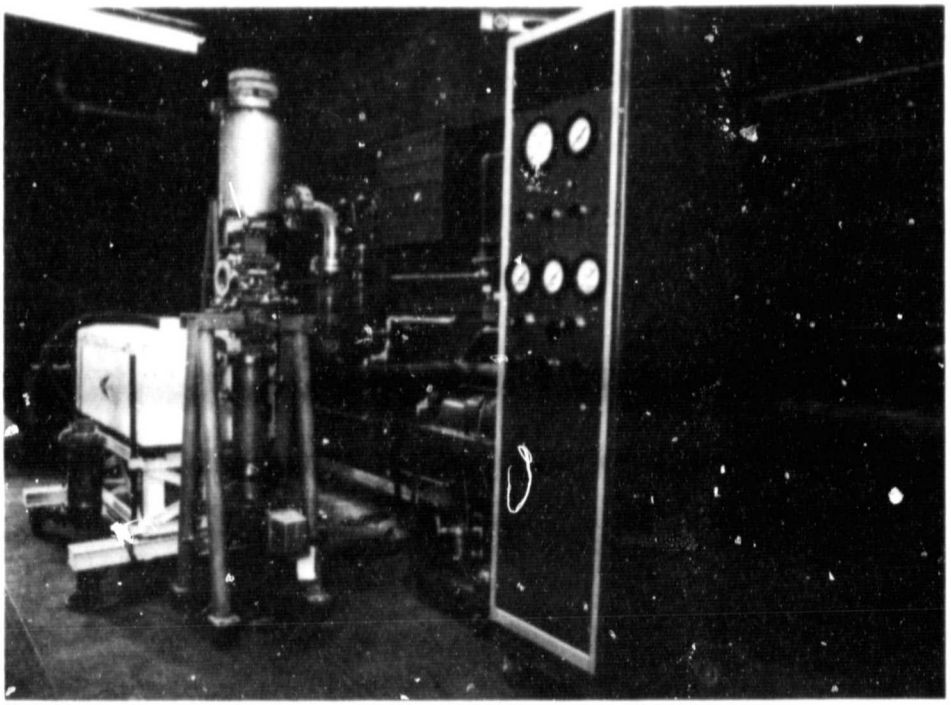

Figure 1. Overview of Cell Showing LDV, Rig, Fuel Cart, and Air and Fuel Control Console

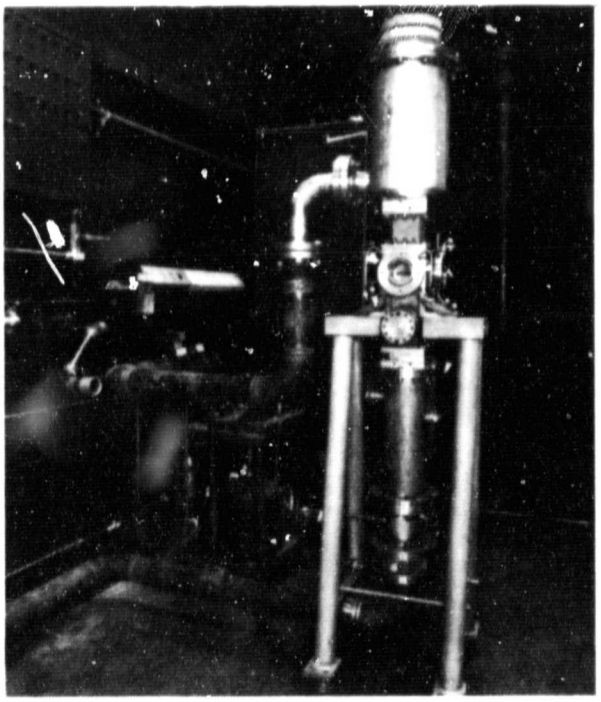

Figure 2. Rig Installed With Inlet and Exhaust Lines

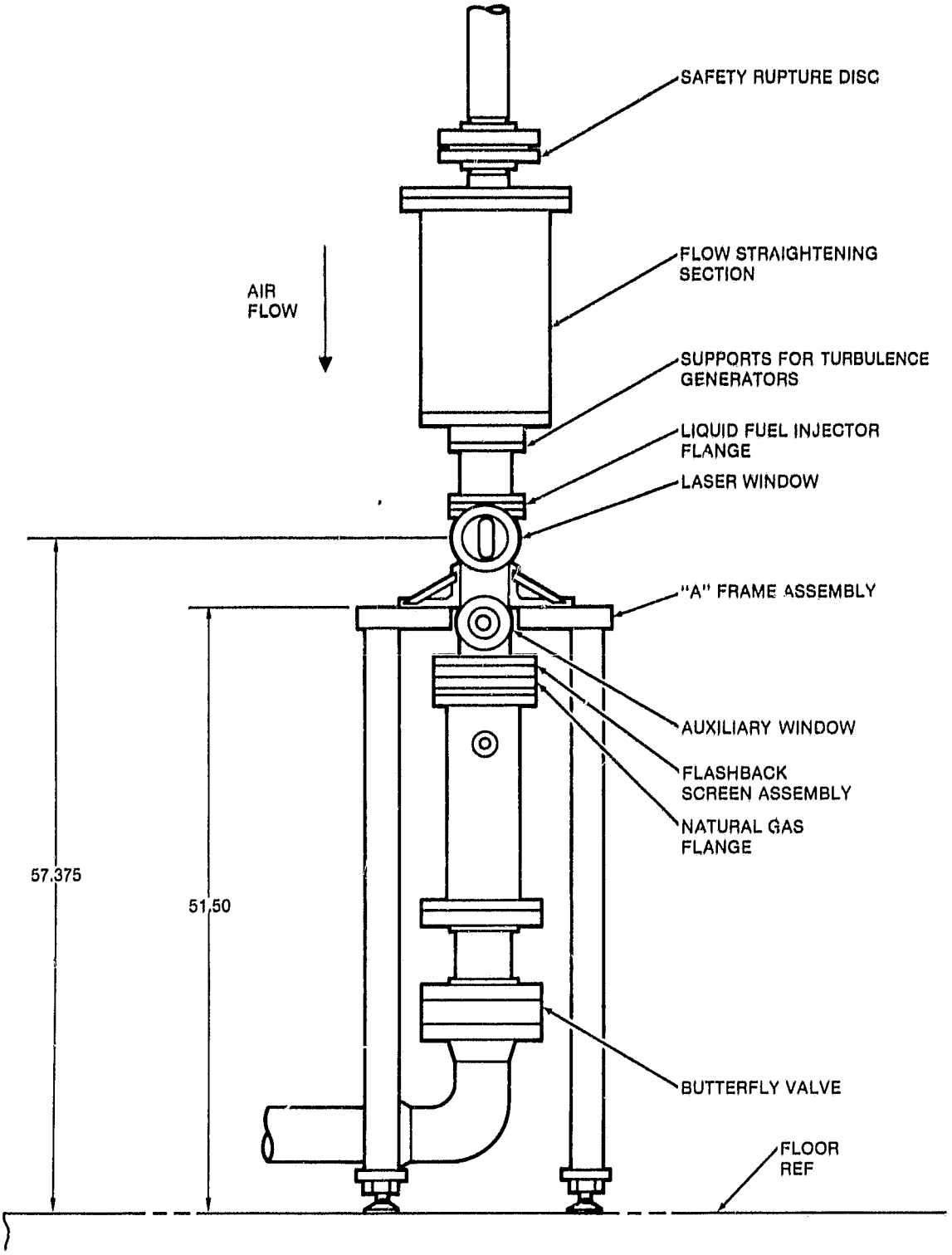


Figure 3. Fuel Atomization Rig Mounted on A-Frame

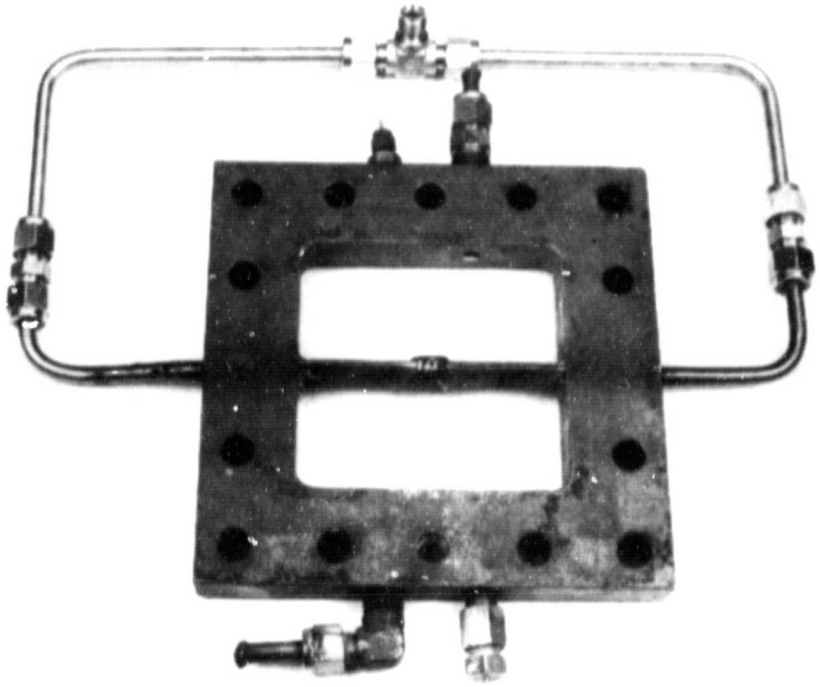

Figure 4. Liquid Fuel Injector Flange Assembly

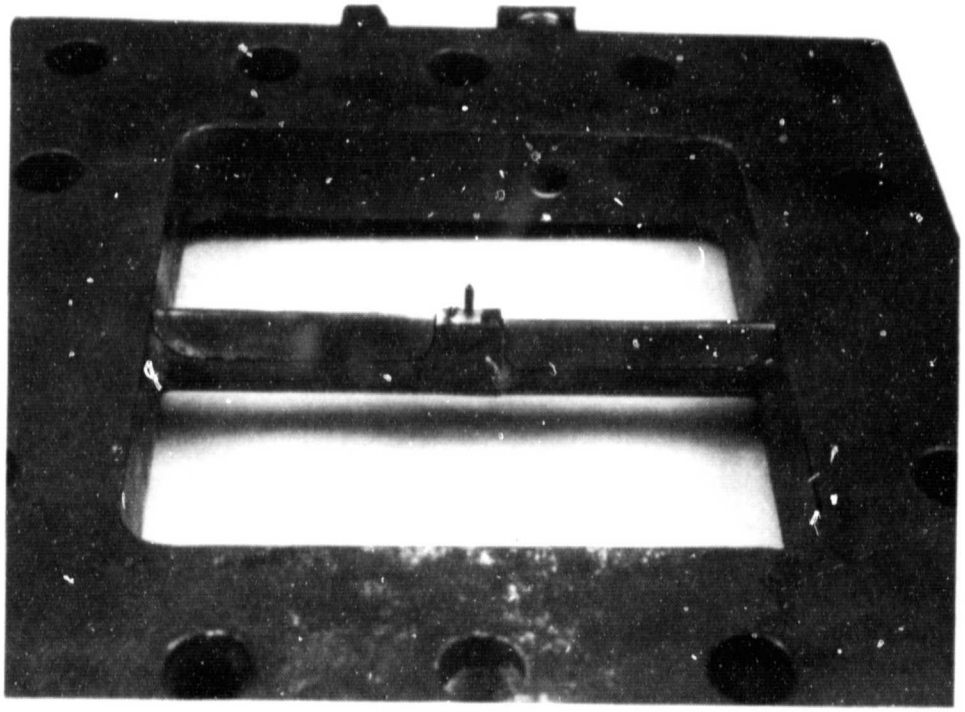

Figure 5. Closeup of Fuel Injector Nozzle

The laser measurement section is the most complex assembly in the rig. It is pictured in Figures 6 to 10. This section includes the laser beam window and ports, the laser beam dump, the off-axis detector window and ports and two auxiliary optical port for other instrumentation. To prevent major flow disturbances plates were installed flush with the inner walls of the flow path at each measurement section. Slots were machined in these plates prior to the optical measurements. The laser measurement section contains pressure and temperature instrumentation. The beam dump port served the additional purpose of being a port for instrumentation rakes.

The afterburner section (Fig. 11) contains the torch ignitor, natural gas pilot cone, dilution and cooling air port, combustor, transition duct (square to round) and water injector for final air cooling.

A standard butterfly valve with an electical actuator was used to cotrol rig backpressure. Because the valve was rated for 427°C service it was necessary to spray considerable quantities of water into the air stream just ahead of the valve. A thermocouple was used to monitor air temperature at the valve.

## 2.3 RIG CONTROL AND CONTROL INSTRUMENTATION

All optical measurements were made at air temperatures of 375°C. Variations over a six hour run were within 2.8°F. Air from high pressure compressors was directed through a heater to achieve the design operating temperature. The flow was controlled by a remotely actuated valve. Flow rates were measured using a standard ASME orifice run.

The fuel subsystem was designed to provide high pressure fuel at the design flowrate of 0.9 kg/s configurations. The fuel was filtered to prevent clogging of the fuel injector.

Nitrogen was used to purge the optical window ports and laser beam dump to maintain clarity. Needle valves were used to adjust nitrogen flow into the flow section. The total nitrogen flow was minimized to reduce the disturbance of the air flow in the measurement section. The primary purpose of this subsystem is to maintain high optical transmission through the quartz windows.

Overall rig instrumentation is detailed in Figure 12. Thermocouples in critical locations were routed to limiting pyrometers. Actual instrumentation channels recorded did not include all instrumentation shown. Many instruments were monitored by the test engineer to insure rig safety and not recorded.

The control panel with instrumentation readouts is shown in Figures 13 to 15.

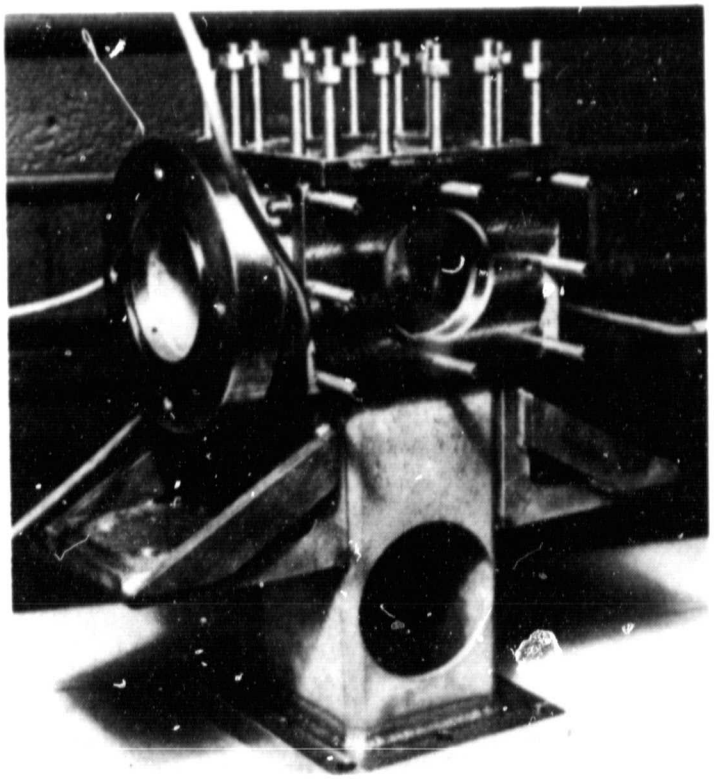

Figure 6.

Laser Measurement Section

(The laser beam dump will be installed in the upper port. Transmissometer ports were welded into the lower ports at the time of these photos.)

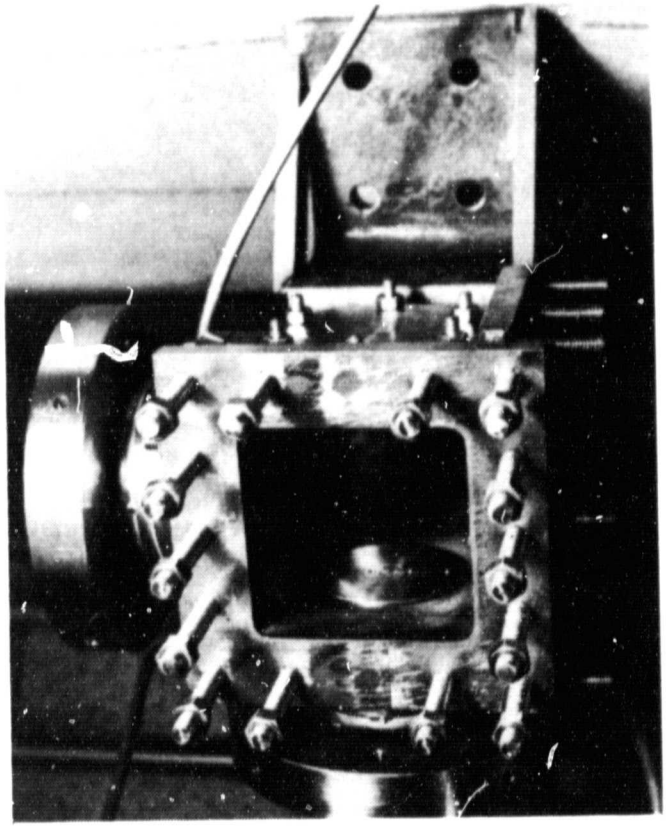

Figure 7.

Top View of Measurement Section

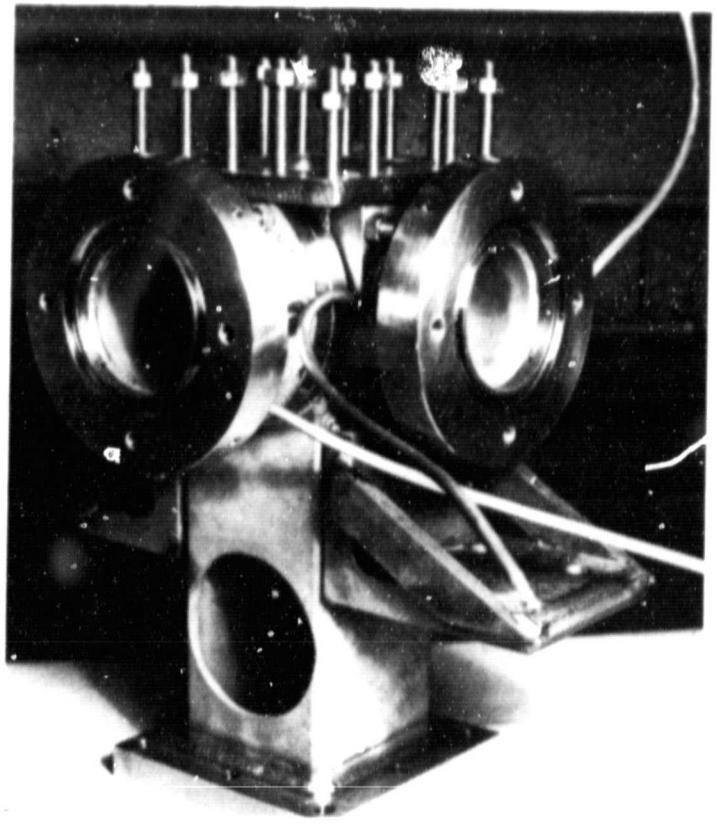

Figure 8.

The Two Measurement Window Flanges Can be Seen in This View of the Measurement Section. (Nitrogen purge tubes are assembled.)

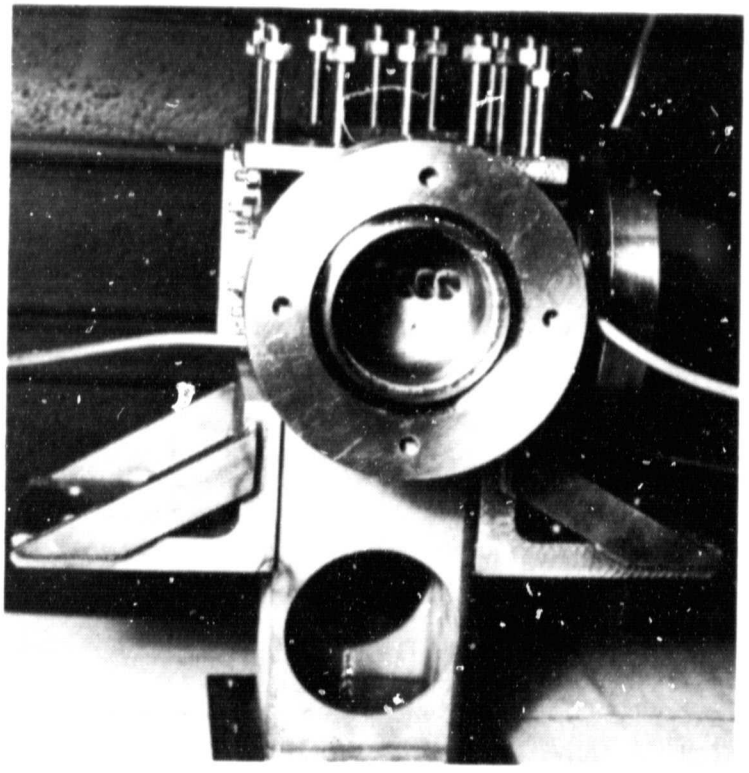

Figure 9.

Apertures for the Laser Beam are Visible Inside Window Flange. (The entire rig is supprted on the brackets extending from both sides.

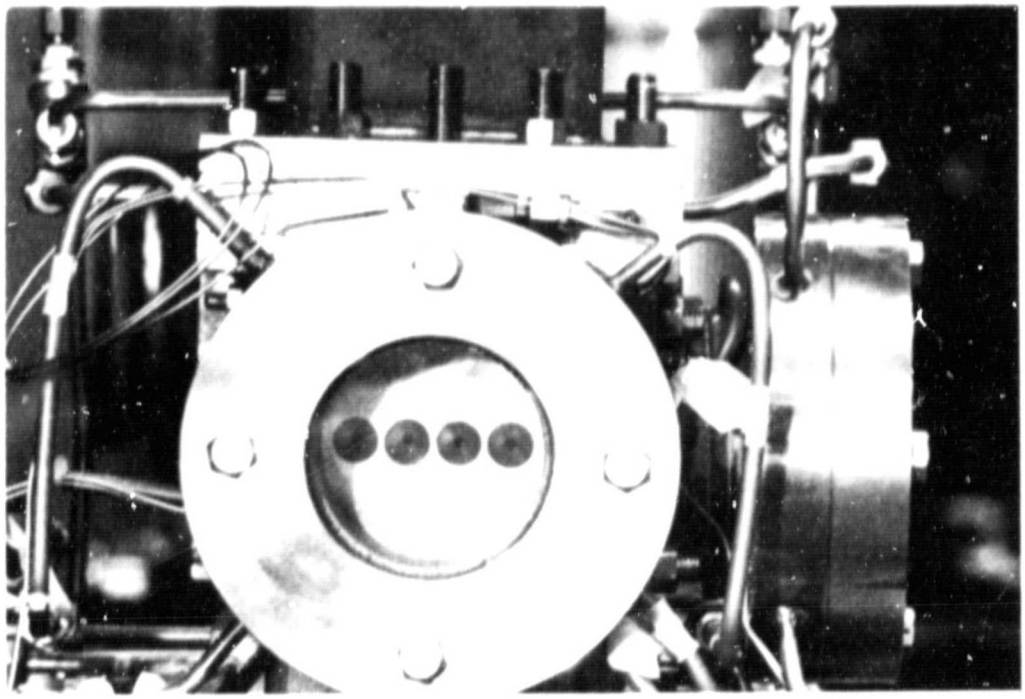

Figure 10. Laser Entry Window With Four Ports

## 2.4 LDV TECHNIQUE

### 2.4.1 LDV Operating Procedure

The techniques used to obtain size and velocity information differed from standard LDV practice in one significant way; the detector measured the scattered laser light 90 degrees off axis (the laser beam defines the axis). This technique provided smaller probe volumes and fewer incidents of multiple droplet measurement. In this technique, two laser beams are used, but only one component of droplet velocity and size are measured at one time. The lens in front of the detector selects the signal from only the central part of the elipsoid created by the intersecting laser beams. In this manner the probability for multiple droplets in the probe volume is considerably reduced. Data can be taken in regions where the drop density is so high that some detection techniques would not provide significant data. There was great concern that the results would be biased if approximately 90 percent of the data were rejected. Since this rejection does not occur with the off-axis detector the bias problem was reduced considerably.

SDL was subcontracted to take optical data using their equipment. Spectron set up the equipment at Solar in early September 1979. That equipment is

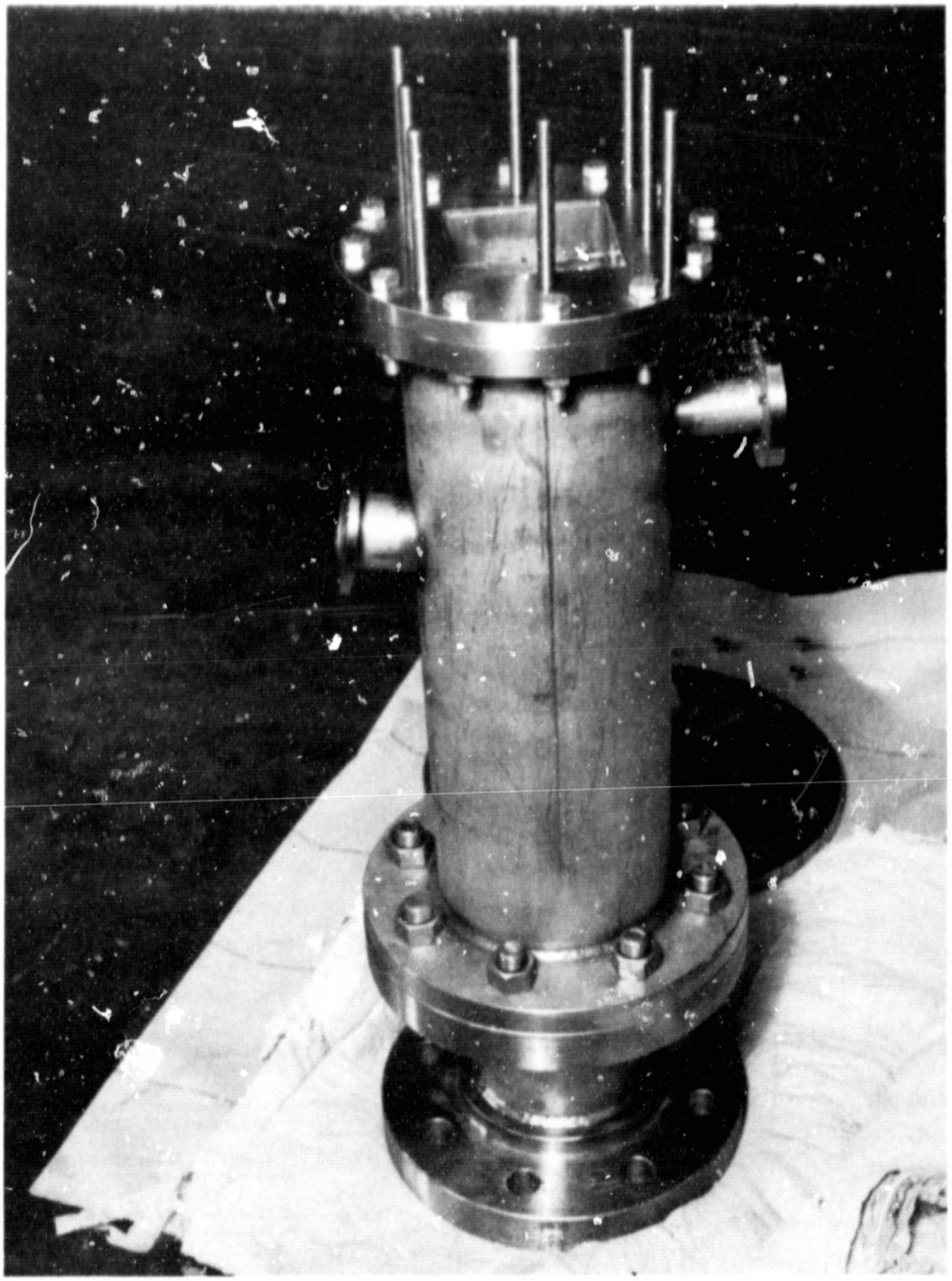

Figure 11. Afterburner Section. (Torch ignitor port is on the left while cooling air is introduced via the port on the right.)

represented in the sketch in Figure 16 and shown photographically in Figures 17 and 18. The data consist of size and velocity measurements of fuel droplets and the surrounding air.

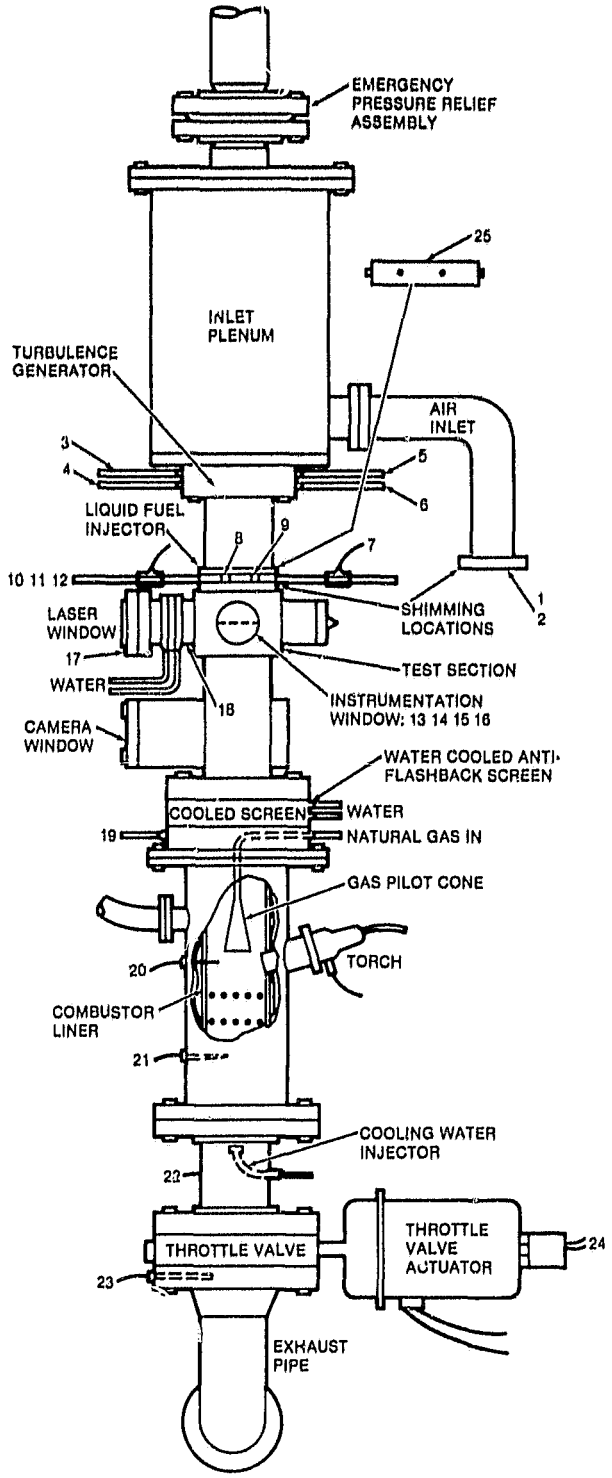


NOTES. (* MEANS INITIALLY CRITICAL)

* 1 $\Delta P_0$ ORIFICE PRESSURE DROP. HEATED AIR SUPPLY (1), $\Delta P$ TRANS.
* 2 $T_0$, ORIFICE AIR TEMP., HEATED AIR SUPPLY (1), P.R.T.

3 $T_1$ (1), P.R.T.

4 AND 5, STATIC PRESS. $\Delta P_{15}$ (1), AND $P_{15}$ 4, BOTH: TRANSDUCERS

6 $P_{11}$, (1), TOTAL PRESSURE, TRANS.

* 7 $T_{F\text{-}IN}$, $T_{F\text{-}OUT}$, (1 OF EACH), FUEL TEMP. P.R.T.'S.
* 8 $P_{2S}$, WALL TAPS IN FUEL BLOCK, (2), PRESSURE TRANSDUCERS
* 9 $T_2$, (2), C.A. THERMOCOUPLES IN FUEL BLOCK
* 10 $N_{F1}$ $N_{F2}$, (1 OF EACH) LIQUID FUEL TURBOFLOWMETER COUNTS FROM FUEL CART
* 11 $T_{F1}$, $T_{F2}$, (1 OF EACH) FUEL PRESS. ON CART, PRESS. TRANSDUCER.
* 12 $P_{F1}$, $P_{F2}$, (1 OF EACH) FUEL PRESS. ON CART. PRESS. TRANSDUCER
* 13 $P_{35}$, WALL TAPS IN LASER PLANE, (2) ONTO PRESSURE TRANSDUCERS
* 14 T3A, WALL MAGPACKS (C.A. THERMOCOUPLES) (2)

15 $P_{3t}$, ARRAY OF 24 ON REMOVABLE PLUG, TOTAL PRESSURE, TRANS.

16 T3B, ARRAY OF 13 ON REMOVABLE PLUG, C.A. THERMOCOUPLES

17 $T_W$, WINDOW FLANGE TEMP. (2), C.A. THERMOCOUPLES

18 $P_W$, WINDOW N2 BUFFER PRESS. ONTO $\Delta P$ GAGE WITH $P_{35}$.

19 $T_4$ (1), FLASHBACK INDICATOR; C.A. THERMOCOUPLE ONTO PYROM.

20 $T_5$ (1), C.A. THERMOCOUPLE ONTO PYROMETER, OPTIONAL TO 20

22 $T_7$ (1), C.A. THERMOCOUPLE ONTO PYROMETER

23 $P_{ES}$, EXHAUST STATIC PRESSURE, GAGE

24 THROTTLE VALVE POSITION INDICATOR ONTO PANEL METER

25 INSTRUMENTED BLOCK, $P_{2T}$ (6) KIEL PROBES $P_{2S}$ (2) WALL TAPS, AND $T_2$ (8) C.A. THERMO.S

Figure 12. Liquid Fuel Premix Rig Instrumentation

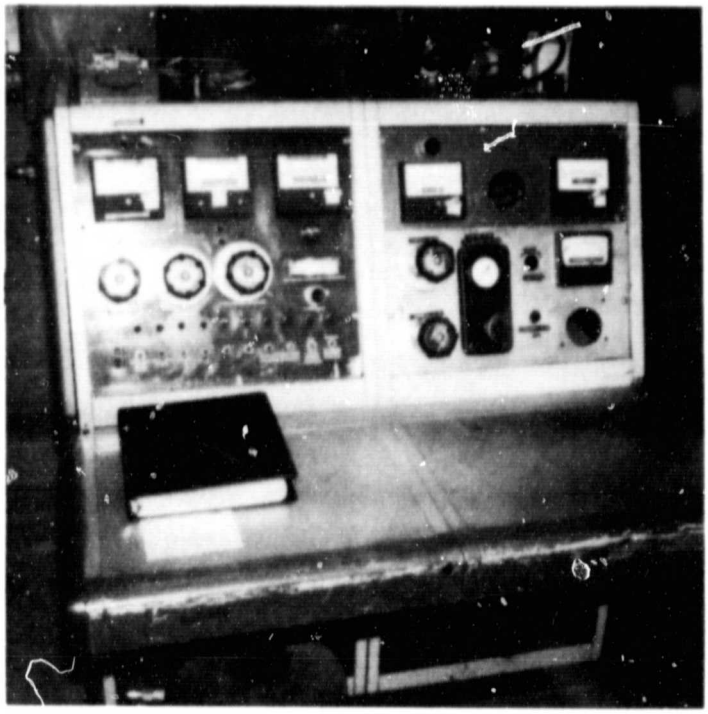

Figure 13. Main Control Panel for Test Rig

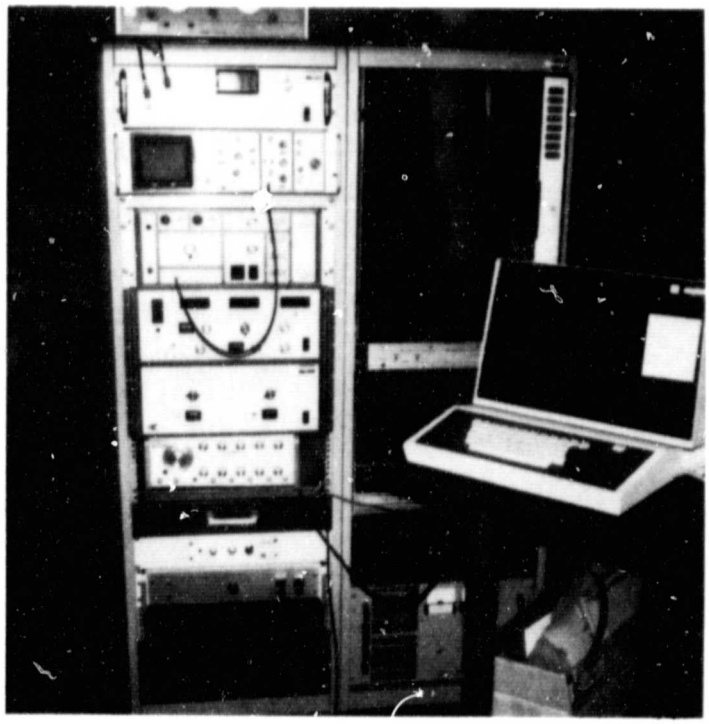

Figure 14. LDV Signal Conditioning and Control

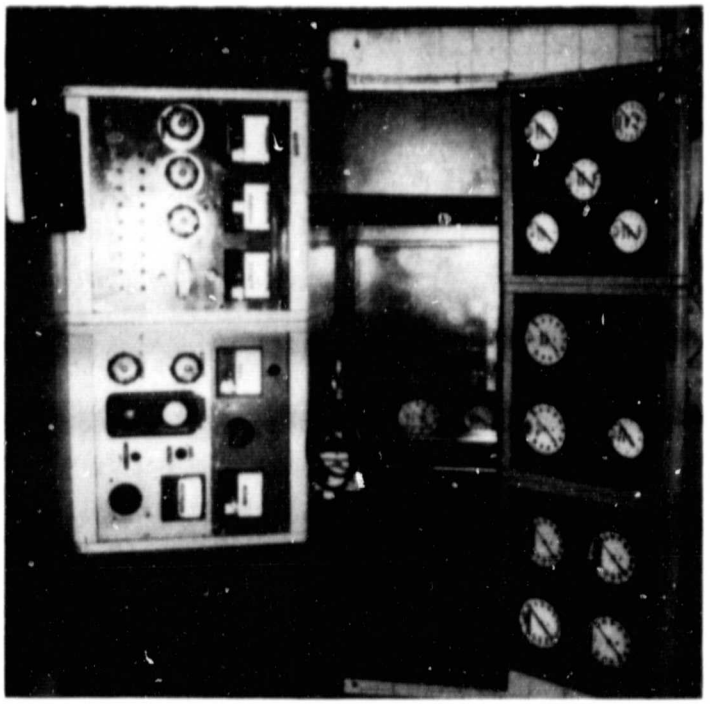

Figure 15. Overall Control Panel With View Into Test Cell

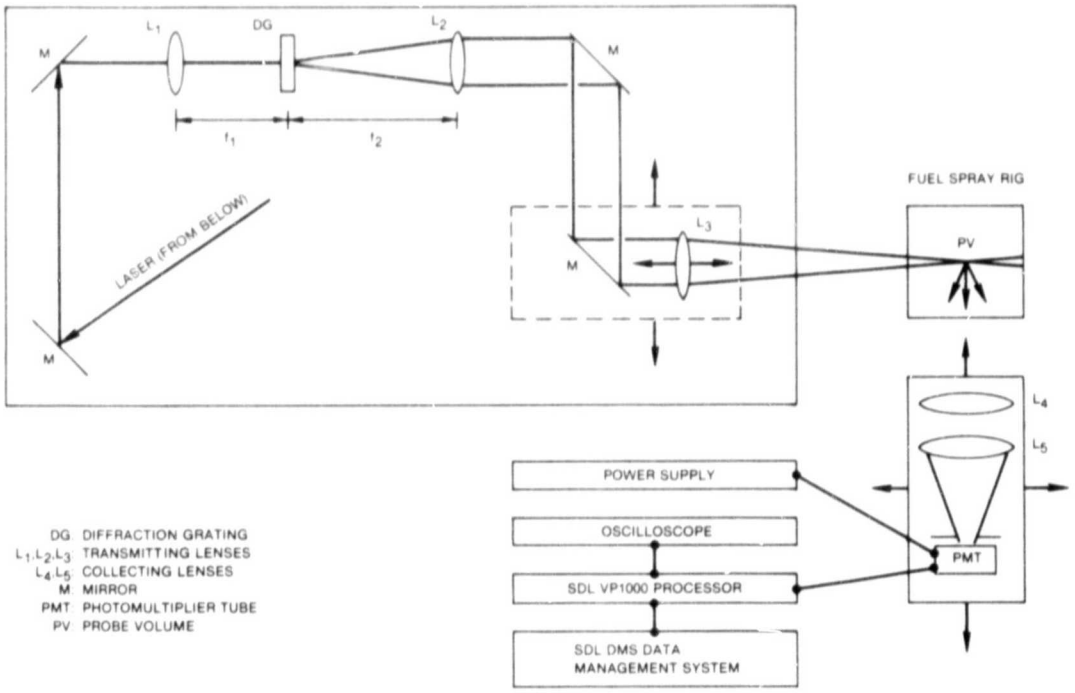


Figure 16. Diagram of SDL Equipment for Off-Axis Measurement

ORIGINAL PAGE IS
OF POOR QUALITY

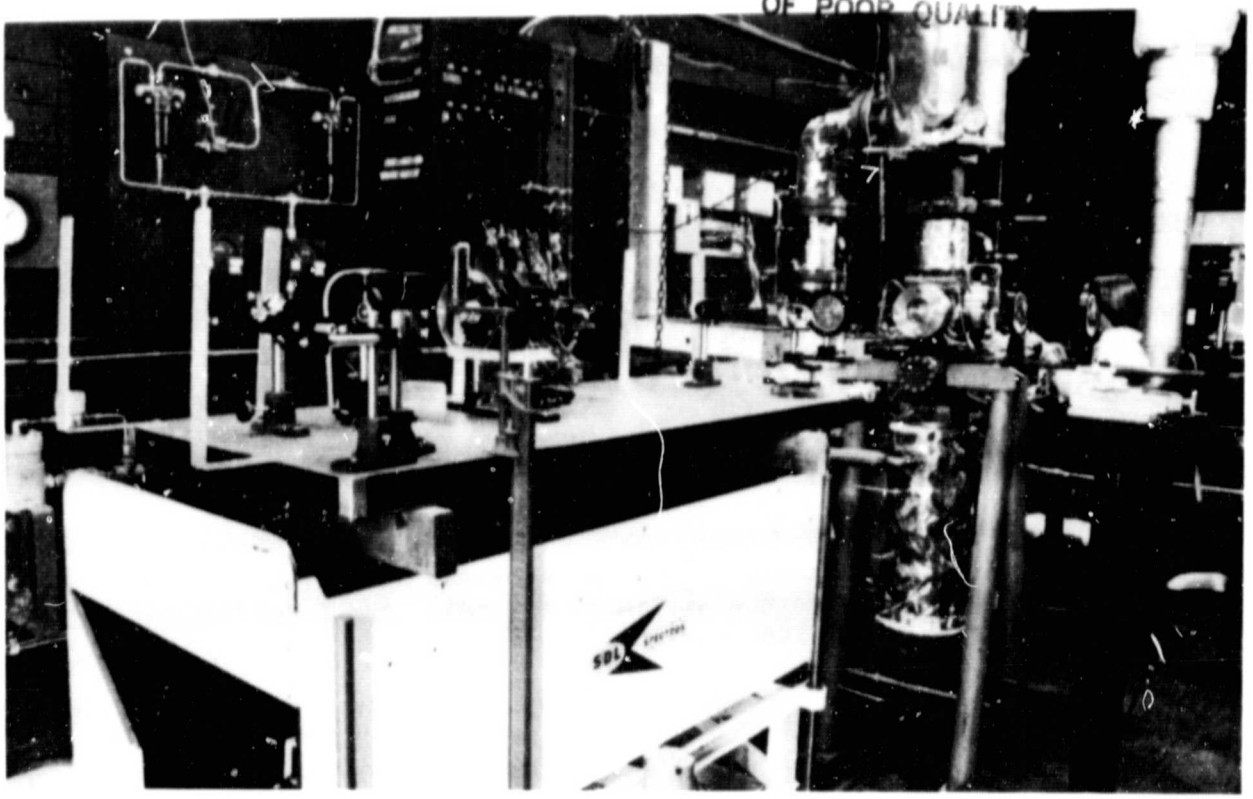

Figure 17. Optical Bench for SDL Tests

Figure 18. Signal Processor for SDL Tests

Two types of measurements were made: visibility and Doppler period (see Appendix A for description). These were then converted to size and velocity of individual particles or droplets. From this information, several important parameters were then obtained. They are: linear mean diameter, size standard deviation, surface mean diameter, kurtosis, mean velocity, and turbulence intensity. These parameter as defined below.

In an effort to understand the interaction between the fuel droplets and the surrounding air, the velocities of both media were measured. The velocity of the air was obtained by seeding it with 3 $\mu$m glass beads using a fluidized bed and subsequently measuring the bead velocity.

### 2.4.2 LDV Data Recording Procedure

The positions where the measurements were taken are identified by the indices (i,j) where i corresponds to the abscissae (x) axis, and j corresponds to the ordinate (y) axis as specified in Figure 19.

The data of each task are presented in matrix form where the position, mean velocity, turbulence intensity, and linear mean diameter are specified. In the SPRAY series, the velocity and size distributions are also provided.

The heading of the test data matrix indicates the series and the position of the run. For instance, SPRAY 1 RUN 2-1 indicates that the measurements were taken at 30 cm plane and the position 2,1). The histogram that follows, plots the frequency of the particle of a certain size versus the corresponding size. This frequency is obtained by dividing the number of particles of a certain size by the total number collected. That is, frequency fi = $N_i/N$. The maximum frequency of the ordinate is then indicated. Typically, it is 0.1. The ordinate is then divided into five equal numbers of intervals.

The table below the graph shows the values that were used to construct the graph: the diameters of the particles and the number of particles with this diameter (count). Finally, there is a list of the size and velocity parameters of interest for this test.

The next graph shows the velocity versus size distribution. The maximum velocity (ordinate) is indicated, and again the ordinate is divided into five equal intervals. The table below indicates the velocity and turbulence intensity corresponding to each size.

The data and graphs are included in Section 3.

### 2.4.3 Definition of Size and Velocity Parameters

Let:

$D_i$ = diameter of droplet i,

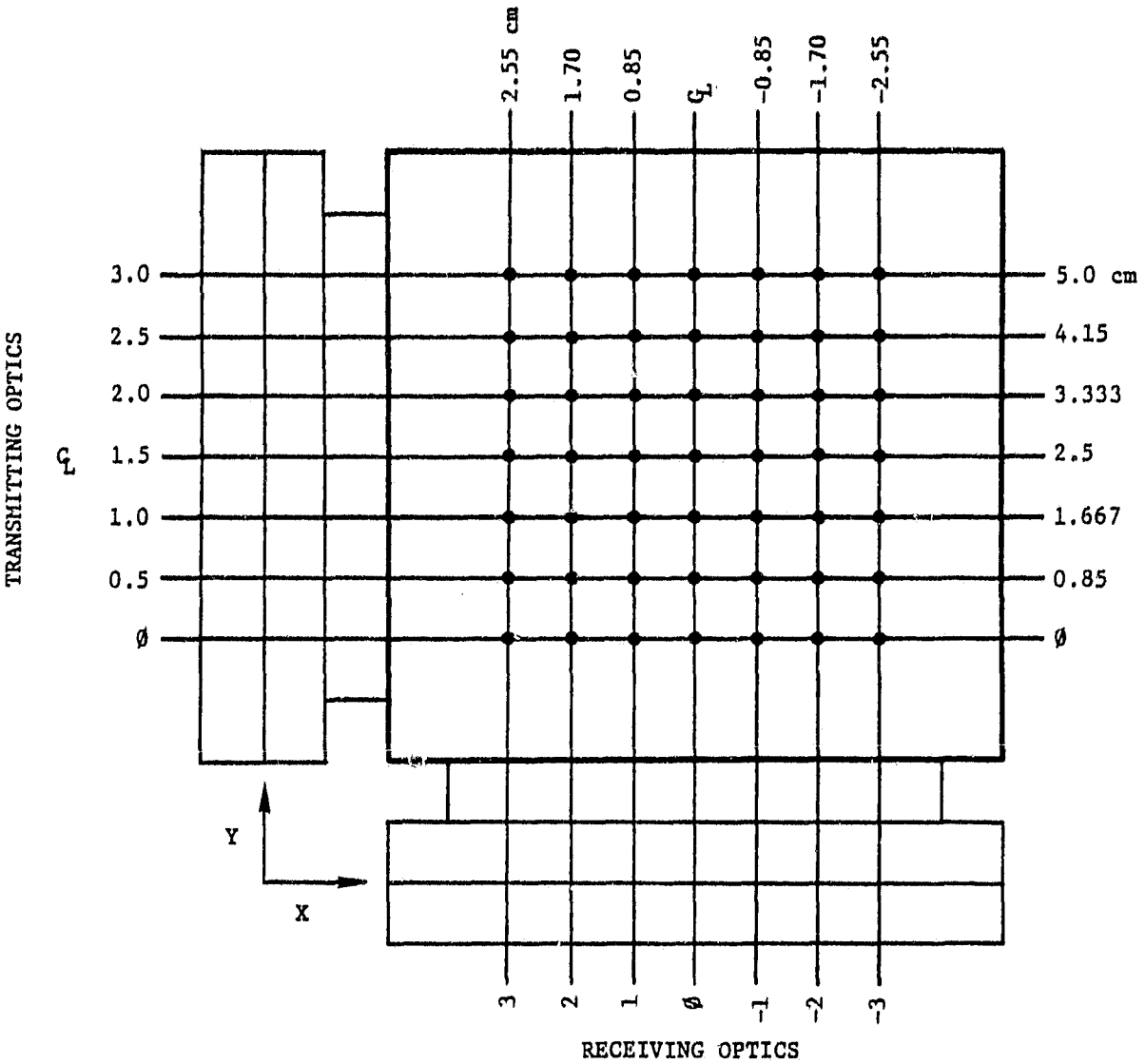


SERIES: SPRAY 1 - 30 cm DOWNSTREAM NOZZLE PLANE
SPRAY 2 - 15 cm DOWNSTREAM NOZZLE PLANE
SPRAY 3 - 7.5 cm DOWNSTREAM NOZZLE PLANE

RUN : 16/PLANE AT LOCATIONS (REC, TRANS)

Figure 19. Test Matrix

$N_i$ = number of i droplets collected,
$U_i$ = velocity of droplet i, and
$N$ = total collected droplets + $\Sigma N_i$.

The following can then be defined:

Linear mean diameter: $D10 = \Sigma N_i D_i / N$ ,

Surface mean diameter: $D20 = [\Sigma N_i D_i^2 / N]^{1/2}$ ,

Volume mean diameter: $D30 = [\Sigma N_i D_i^3 / N]^{1/3}$ ,

Sauter mean diameter: $D32 = \Sigma N_i D_i^3 / \Sigma N_i D_i^2$ ,

Standard deviation: $S = [\Sigma N_i (D_i - D10)^2 / N]^{1/2}$ ,

Kurtosis: $\Sigma N_i (D_i - D10(_3 / N \ / \ [\Sigma N_i (D_i - D10)^2 / N]^{3/2}$ .

Mean velocity: $\bar{U} = \Sigma N_i U_i / N$ ,

Turbulence intensity: $T = [\Sigma N_i (U_i - \bar{U})^2 / N]^{1/2} \ / \ \bar{U}$ .

## 2.5 SPECIAL INSTRUMENTATION

Several special instrumentation probes were built to measure the performance of the rig prior to the fuel droplet measurements. Data obtained from the probes are presented in Section 3.

### 2.5.1 Temperature Uniformity in Measurement Plane

The optical droplet measurements were made in a plane perpendicular to the flow axis. That plane was called the measurement plane. Air temperature and pressure measurements were made in that plane to assure uniformity.

An instrumentation rake was built to install in the rig at the measurement plane. It contained 13 thermocouples to measure total gas temperature. The thermocouples were arranged in a cross pattern (see Fig. 20). They were routed through a cruciform shaped airfoil to reduce the disturbance of the air flow.

### 2.5.2 Fuel Injection Plane Measurement Probe

A probe was designed to measure pressure and temperature at the fuel injection plane. The basic design is shown in Figure 21. This probe was installed in a spool section and replaced the fuel injector module. The probe spool piece was equipped with wall pressure and temperature probes.

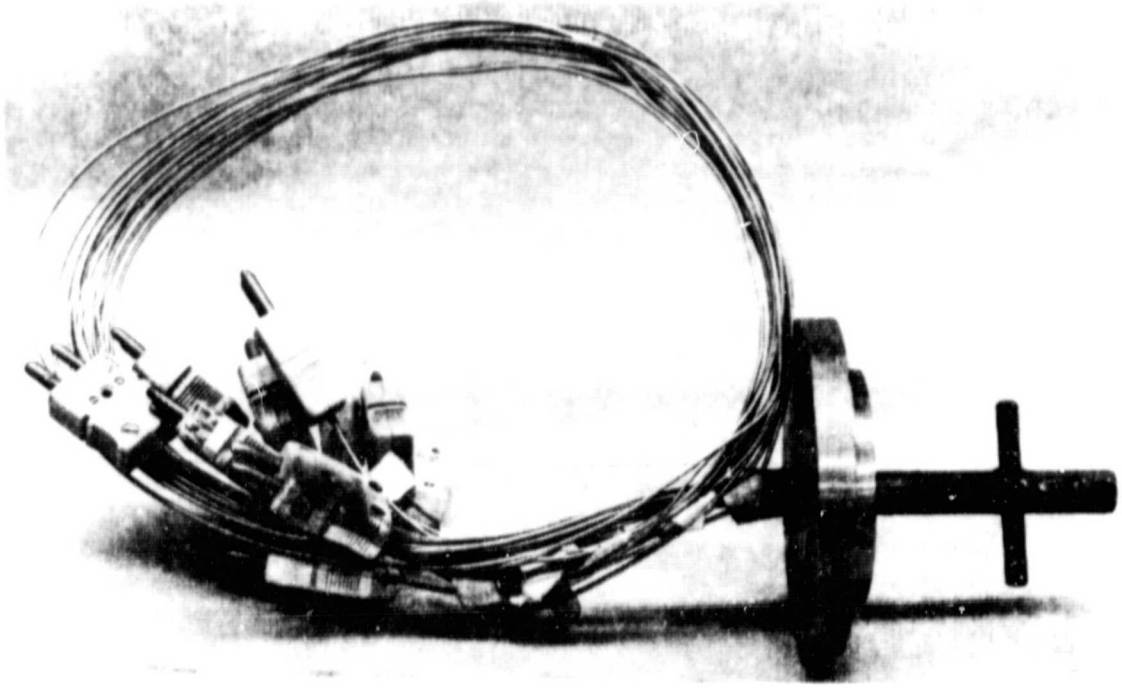

Figure 20. Measurement Plane Probe

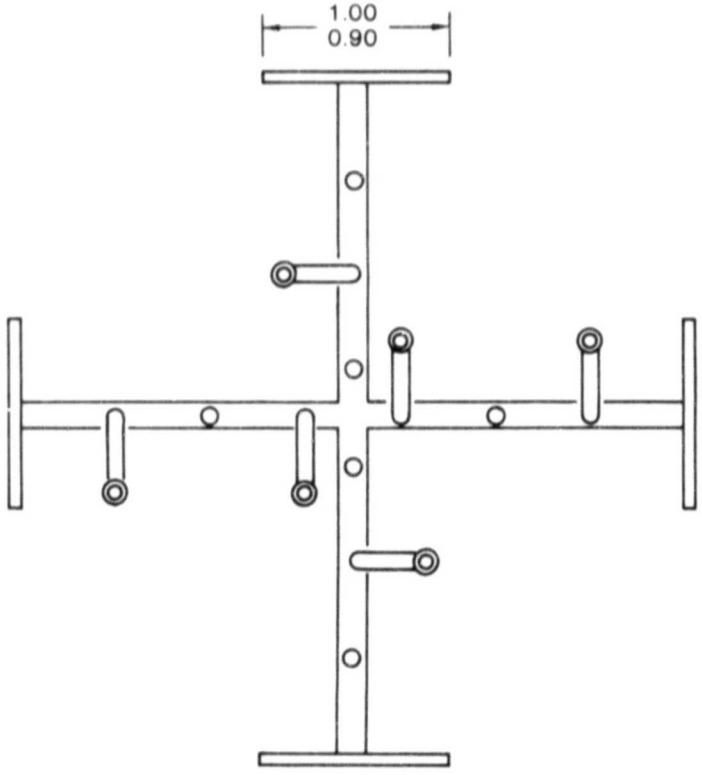


Figure 21. Pressure/Temperature Probe for Fuel Plane

### 2.5.3 Probe for Flow Uniformity and Spillover Measurements

A sampling probe was designed and built for the flow uniformity and spillover measurements. The probe replaced the laser beam dump and received samples of the air or air/fuel mixtures at the laser measurement plane. Six samples could be made with the rig at operating conditions without moving the probe. The probe could be positioned into a total of four slots to achieve the 24 point grid (Fig. 22).

In order to measure the percent of fuel vaporized in the measurement plane Solar followed the technique of Tacina[1]. A catalytic reactor was built which was patterned after a design supplied by NASA. The catalyst used was 0.5 percent Pt on Gamma Alumina. The basic design was reasonably successful with problems occurring only in the heater. The electric heater element for the reactor was manufactured straight. To fit the reactor, the element was wound into a helical shape and inserted into the shell. The actual bend radius was smaller than that tolerated by the element resulting in an open circuit failure after each cycle. The design was altered by removing the strip heater and surrounding the core with a clamshell heater.

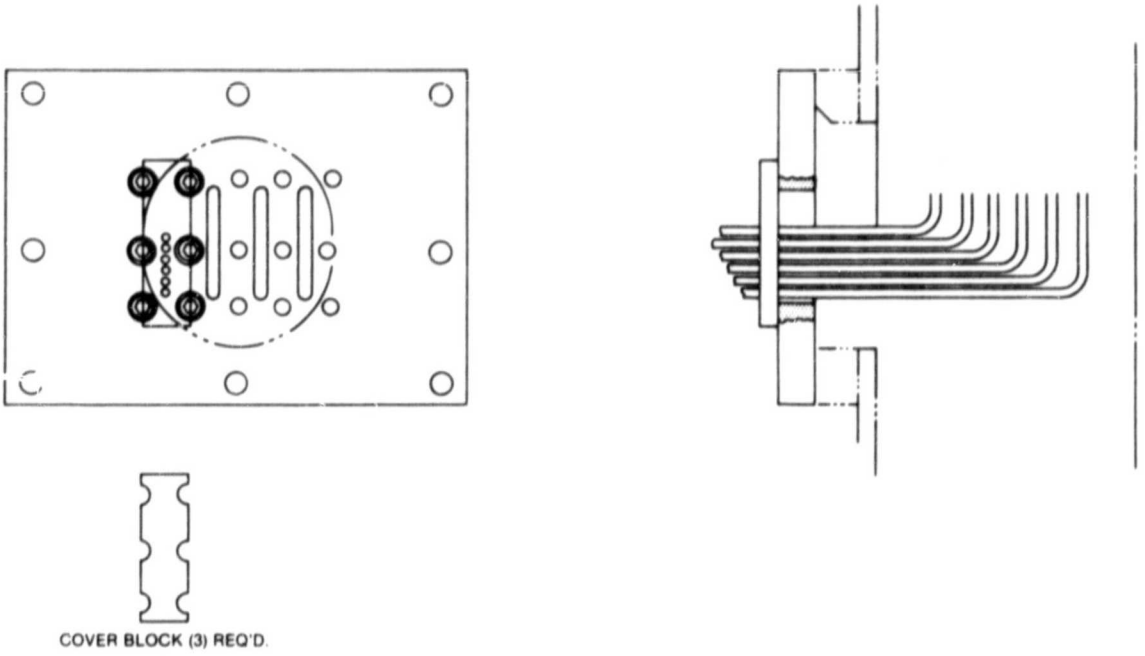


Figure 22. Sampling Probe

[1]Tacina, Robert R., "Degree of Vaporization Using an Airblast Type Injector for a Premixed-Prevaporized Combustor", NASA TM-78835, presented at First International Conference on Liquid Atomization and Spray Systems, Tokyo, Japan, August 28-31, 1978.

## 2.6 FUEL EVALUATION TESTS

All fuel used during this study was drawn from a single 3800 l tank. Only this program used the fuel in that tank. The tank was pumped empty and then filled with commercial Jet A at the beginning of the test in June 1979. A sample of that fuel was taken on three separate occasions and tested in the Solar Chemistry Laboratory. The results of those three evaluations are shown in Table 1. There is some variation in the measured properties and these cannot be explained fully. It is possible that some fuel evaporation occurred between the first test and the subsequent two evaluations. The test rig had not been operated for a period of months when the third evaluation was made. A complete distillation curve was not measured during the second test. All chemistry testings were performed by the same personnel using the same equipment and techniques.

Table 1

Fuel Sample Evaluation

| | #1 7/79 | #2 11/79 | #3 4/80 | Units |
|---|---|---|---|---|
| Kinematic Visocisty | 1.55 | 1.46 | 1.55 | (centistokes @ 100°F) |
| Gravity | 43.2 | 43.7 | 40.3 | Degrees API @ 60°F |
| Pour Point | -80 | -72 | 88.6 | °F |
| Flash Point | 140 | 170 | 160 | °F |
| Distillation BP | 357 | | 356 | °F |
| 10 | 390 | | 379 | °F |
| 20 | 403 | | 386 | °F |
| 50 | 430 | | 409 | °F |
| 90 | 484 | 455 | 460 | °F |
| End PT | 548 | 505 | 510 | °F |
| % Recovery | 98.5 | 98 | 95 | % |
| Carbon Residues | 0.28 | 0.08 | 0.095 | % |

# 3

# MEASUREMENTS

The results presented in this section are divided into two sections; measurements of the rig flow characteristics without fuel droplets, and measurements concerning droplets in that flow field.

## 3.1 PRELIMINARY RIG MEASUREMENTS

This subsection describes the measurements of the flow temperature and uniformity of the rig without fuel being present. (The inlet air was preheated in an external heat exchanger.)

### 3.1.1 Temperature Uniformity

The air temperature was measured at the optical (LDV) measurement plane using the probe described in Section 2.5.1. The conditions for that test were:

- air temperature 744K
- air pressure 507 kPa
- reference velocity 40 m/sec

No fuel was injected during this test. The data from the thermocouples is shown in Table 2. The thermocouple numbers are referenced in Figure 23.

One thermocouple failed, but the remainder indicated that an extremely uniform temperature distribution in the measurement plane had been achieved.

Temperatures were also measured at the fuel injection plane using the probe described in Section 2.5.2. The conditions at the time of that test were:

- air temperature 650K (nominal)
- air pressure 507 kPa
- reference velocity 40 m/sec.

Data from that test are shown in Figure 24. The mean temperature was 656K with a standard deviation of 0.44K.

Table 2

Thermocouple Data

| Thermocouple Number | Temperature (°K) |
|---|---|
| 1 | 741 |
| 2 | 741 |
| 3 | Failed |
| 4 | 741 |
| 5 | 741 |
| 6 | 741 |
| 7 | 741 |
| 8 | 742 |
| 9 | 741 |
| 10 | 741 |
| 11 | 742 |
| 12 | 742 |
| 13 | 742 |

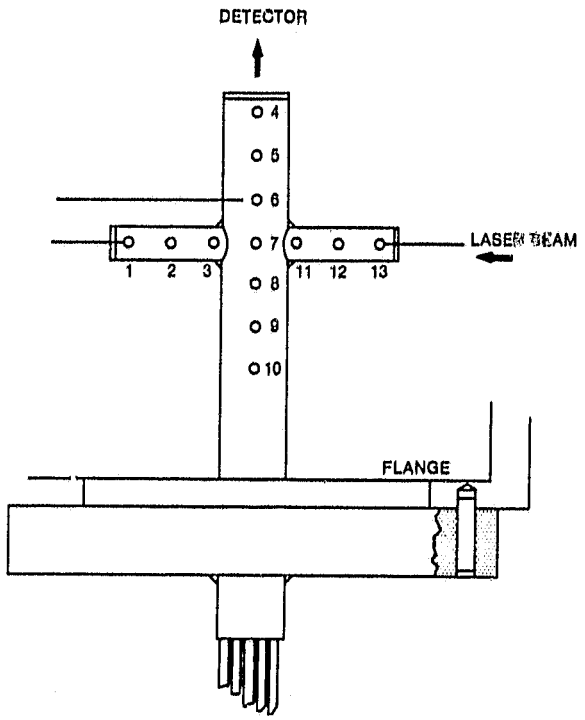


Figure 23. Diagram of Measurement With Thermocouple Numbers

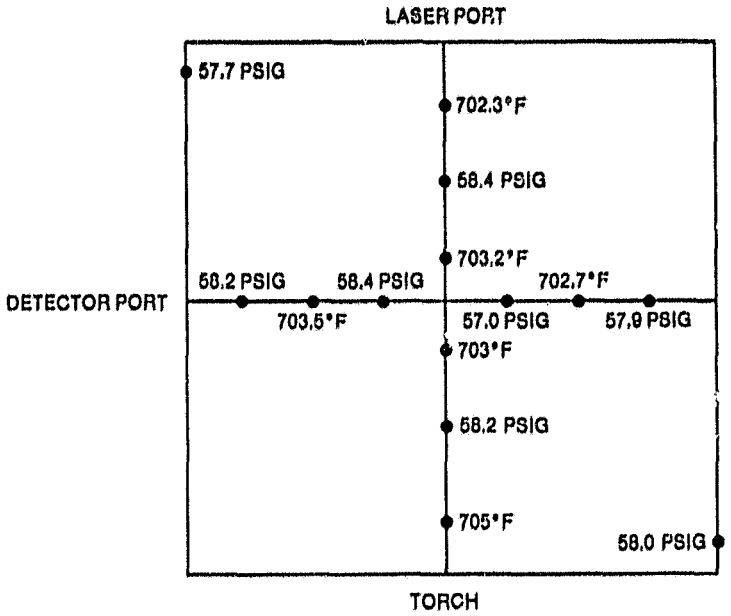


Figure 24. Temperature and Pressure in Fuel Plane

### 3.1.2 Flow Uniformity

The uniformity and symmetry of the air flow in the mixing section was determined by injecting methane into the rig at a point in the center of the fuel injection plane. A probe (Fig. 25) was constructed in a square spool piece which replaced the fuel injector. Methane was injected into rig while the rig was being operated at

- Air temperature 650K
- Air pressure 5 atm
- Reference velocity 40 m/s

A sampling probe (Fig. 22) was constructed for use at the measurement plane. The rectangular mounting plate of that probe replaced the laser beam dump, 180 degrees opposed to the laser port. Each of the six probes could be sequentially attached to a hydrocarbon analyzer. When the rig was shut down the probe could be moved to any of four different positons. In this manner a grid of 24 measurement points was constructed in the optical measurement plane. Unburned hydrocarbons were measured at each of the 24 points. The methane injector was positioned at three different planes to measure the distribution of the methane at 7.5, 15 and 30 cm downstream of the injector. The results of the 72 point survey are shown in Figure 26. The data indicates that the distribution is slightly skewed toward one side. This is probably a result of a slight skew in the injector. Taking this into account, the concentration profiles show the flow uniformity within the tset section is acceptable. Background levels of $CH_4$ were subtracted out before presentation. The sensitivity of the $CH_4$ measurement is $\pm$ 1 ppm overall range. Data gathering was repeated for the right hand column of the 30 cm plane.

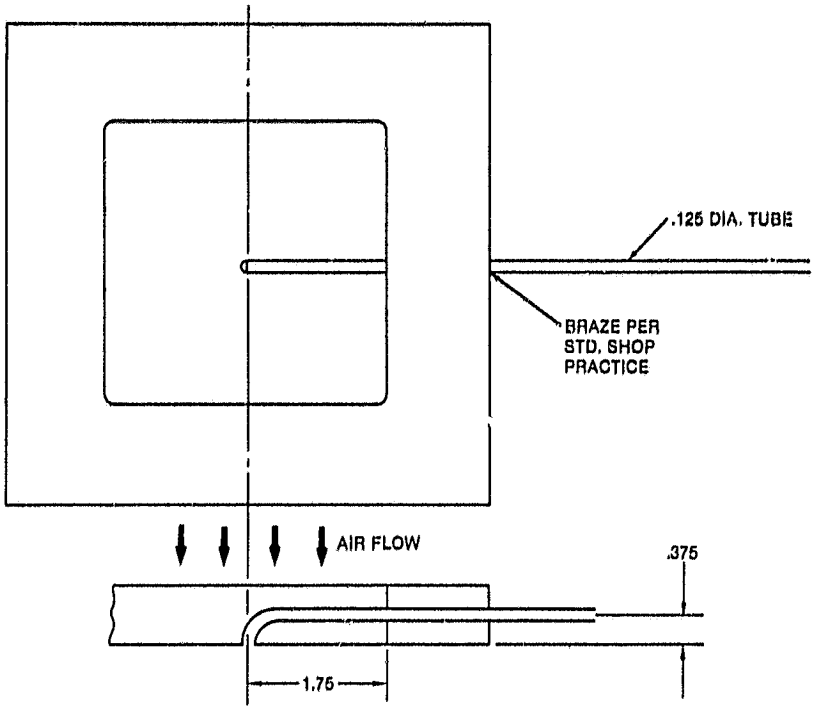


Figure 25. Methane Injection Probe for Flow Uniformity Test

Several pressures were measured at the fuel injection plane using the probe described in Section 2.5.2. The conditions at the time of the test were:

- air temperature 650K
- air pressure 507 kPa (5 atm)
- reference velocity 40 m/sec

The pressure measurements had a mean of 400 kPa (gauge) with a standard deviation of 3.3 kPa. The pressure data sets exhibited good uniformity. The data are shown in Figure 24.

## 3.2 MEASUREMENTS WITH FUEL IN FLOW FIELD

All tests were accomplished with a Jet A fuel and except for one characterization test were performed at one set of operating conditions. These conditions were:

- air temperature = 750K
- air pressure = 75 psia
- air velocity = 40 m/sec
- mean equilibrium ratio = 0.4

The operation set points to achieve these conditions are shown in Table 3. The variations described the tolerance that the rig operator could maintain

Table 3

Set Points for Operating Conditions

| | |
|---|---|
| Inlet temperature | 700°F |
| Rig Pressure | 58.2 psig |
| Orifice Temperature | 727°F |
| Orifice Pressure | 70 psig |
| ΔP Orifice | 11.8 in. Hg |
| Downstream Throttle Temperature | 280°F |
| Fuel flow In | 133 Hz |
| Fuel Flow Total | 88 Hz |
| Nitrogen Window Pressure | 78 psig |
| Fuel Nozzle Pressure | 300 psig |
| Fuel Pump Pressure | 580 psig |
| Cooling Air Pressure | 65 psig |
| Pilot Light Off T.C. | 1700°F |
| Rig Overtemperature T.C. | 450°F |
| Combustor Exit Temperature | In excess of 2200°F |

### 3.2.1 Spillover Measurements

The test were performed in the 7.5 cm measurement plane with the rig at the set position:

- air temperature = 650K
- air pressure = 5 atm
- reference velocity = 40 m/s
- equivalence ratio = 0.4

The probe shown in Figure 22 was used to collect the samples. This probe was used only in the middle two of the four possible positions. This was done primarily because of the narrow spray angle and the proximity of the probe to the fuel injector. The sample location numbering grid is shown in Figure 27.

The conditions of the rig and the emissions data received are shown in Table 4 for position B. Rig conditions are only printed out when changes in conditions were recorded. This order of presentation is the order in which the data was taken. The computer code used to generate the results in snown in Appendix B.

Problems were encountered on several occasions. The existance of the problems limited the amount of data available. In some positions, primarily probe positon C, insufficient flow as obtained to go past the isokinetic velocity. High "percent vaporized" numbers resulting from these data are not realistic and are excluded. The raw data are shown in Table 5 and 6.

LASER WINDOW

| | | | | |
|---|---|---|---|---|
| | 3 | 20 | 8 | 0 |
| | 85 | 315 | 62 | 0 |
| 7.5 CM PLANE | 175 | 640 | 180 | 9 |
| DETECTOR WINDOW | 200 | 700 | 210 | 8 |
| | 135 | 442 | 100 | 0 |
| | 10 | 37 | 8 | 0 |

| | | | | |
|---|---|---|---|---|
| | 130 | 225 | 125 | 15 |
| | 195 | 350 | 208 | 35 |
| 15 CM PLANE | 210 | 390 | 220 | 40 |
| DETECTOR WINDOW | 220 | 400 | 208 | 40 |
| | 210 | 360 | 190 | 35 |
| | 150 | 250 | 130 | 15 |

FLOW UNIFORMITY TEST.

DATA IS PPM OF $CH_4$ AT EACH LOCATION WITH BACKGROUND SUBTRACTED OUT.

| | | | | |
|---|---|---|---|---|
| | 145 | 200 | 140 | 43 |
| | 170 | 215 | 140 | 52 |
| 30 CM PLANE | 175 | 220 | 130 | 47 |
| DETECTOR WINDOW | 180 | 215 | 125 | 49 |
| | 180 | 210 | 128 | 55 |
| | 155 | 185 | 110 | 54 |

TORCH

Figure 26. Flow Uniformity Test Results

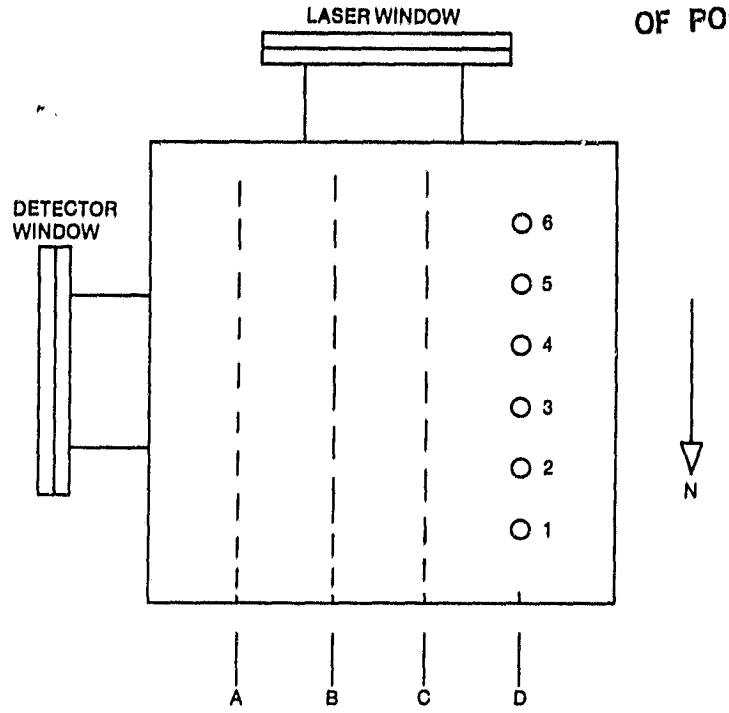


Figure 27. Probe Numbering When Viewed from Top of the Rig

### 3.2.2 Description of Graphs and Tables

The data of the various series is presented in matrix form. The numbers indicated in each element correspond to the position, mean velocity, mean droplet diameter, and turbulence intensity, as appropriate. The corresponding positions in the combustor are indicated in Figure 19

### 3.2.3 Data Collection Summary

The velocity, size, and related statistical parameters of the selected conditions studied in this research program are presented in this section.

They are given in entirity in the Comphensive Data Report.

(1) Air Velocity Uniformity Check: 13 points taken along both centerlines of test section at 30 cm plane.

Series: VELOCITY

## Table 4

## Vaporization Data Via spillover Technique

[illegible] FUEL : JET-A

| ORIFICE TEMP F | ORIFICE PRESS PSIG | ORIFICE DELTA P IN HG | RIG TEMP F | RIG PRESS PSIG |
|---|---|---|---|---|
| 700 | 66.0 | 11.0 | 700 | 59.0 |

| FUEL FLOW LB/HR | AIR FLOW LB/HR | FUEL/AIR RATIO | MEAN ISOKINETIC VELOCITY, FT/SEC |
|---|---|---|---|
| 138.4 | 6664.4 | 0.02003 | 129.0 |

SAMPLING LOCATION B-3

| GAS VELOCITY AT PROBE TIP FT/SEC | CO2 % | CO PPM | UHC PPM | F/A RATIO | EQUIVALENCE RATIO |
|---|---|---|---|---|---|
| 127.15 | 5.85 | 5.0 | 14 | 0.03194 | 0.468 |
| 132.47 | 5.47 | 5.0 | 10 | 0.03473 | 0.509 |
| 109.14 | 5.55 | 2.0 | 0 | 0.03256 | 0.580 |
| 97.97 | 5.47 | 6.0 | 8 | 0.04583 | 0.672 |

PERCENT OF FUEL VAPORIZED [illegible]%

| ORIFICE TEMP F | ORIFICE PRESS PSIG | ORIFICE DELTA P IN HG | RIG TEMP F | RIG PRESS PSIG |
|---|---|---|---|---|
| 700 | 66.0 | 12.0 | 700 | 58.5 |

| FUEL FLOW LB/HR | AIR FLOW LB/HR | FUEL/AIR RATIO | MEAN ISOKINETIC VELOCITY, FT/SEC |
|---|---|---|---|
| 138.7 | 6913.3 | 0.02005 | 132.4 |

SAMPLING LOCATION B-4

| GAS VELOCITY AT PROBE TIP FT/SEC | CO2 % | CO PPM | UHC PPM | F/A RATIO | EQUIVALENCE RATIO |
|---|---|---|---|---|---|
| 118.30 | 5.65 | 0.0 | 12 | 0.02644 | 0.388 |
| 125.18 | 5.65 | 0.0 | 10 | 0.02649 | 0.380 |
| 111.69 | 7.02 | 0.0 | 6 | 0.03271 | 0.479 |
| 99.07 | 7.35 | 0.0 | 4 | 0.03608 | 0.541 |
| 97.00 | 5.22 | 0.0 | 5 | 0.02452 | 0.359 |

PERCENT OF FUEL VAPORIZED [illegible]%

SAMPLING LOCATION B-2

| GAS VELOCITY AT PROBE TIP FT/SEC | CO2 % | CO PPM | UHC PPM | F/A RATIO | EQUIVALENCE RATIO |
|---|---|---|---|---|---|
| 57.92 | 1.78 | 0.0 | 6 | 0.00850 | 0.125 |
| 64.29 | 1.78 | 0.0 | 4 | 0.00850 | 0.125 |
| 111.09 | 1.85 | 0.0 | 2 | 0.00880 | 0.130 |
| 98.62 | 2.24 | 0.0 | 12 | 0.01067 | 0.156 |

**Table 4 (Continued)**

PERCENT OF FUEL VAPORIZED
87.765

| ORIFICE TEMP F | ORIFICE PRESS PSIG | ORIFICE DELTA P IN HG | RIG TEMP F | RIG PRESS PSIG |
|---|---|---|---|---|
| 720 | 66.0 | 11.8 | 720 | 59.5 |

| FUEL FLOW LB/HR | AIR FLOW LB/HR | FUEL/AIR RATIO | MEAN ISOKINETIC VELOCITY, FT/SEC |
|---|---|---|---|
| 137.8 | 6802.0 | 0.02026 | 130.7 |

SAMPLING LOCATION B-5

| GAS VELOCITY AT PROBE TIP FT/SEC | CO2 % | CO PPM | UHC PPM | F/A RATIO | EQUIVALENCE RATIO |
|---|---|---|---|---|---|
| 242.81 | 1.26 | 0.0 | 11 | 0.00609 | 0.088 |
| 177.23 | 1.25 | 0.0 | 8 | 0.00603 | 0.088 |
| 108.31 | 1.24 | 0.0 | 7 | 0.00641 | 0.094 |
| 48.83 | 1.57 | 0.0 | 5 | 0.00750 | 0.110 |

PERCENT OF FUEL VAPORIZED
88.572

SAMPLING LOCATION B-6

| GAS VELOCITY AT PROBE TIP FT/SEC | CO2 % | CO PPM | UHC PPM | F/A RATIO | EQUIVALENCE RATIO |
|---|---|---|---|---|---|
| 252.11 | 0.31 | 0.0 | 8 | 0.00149 | 0.022 |
| 112.65 | 0.43 | 0.0 | 5 | 0.00207 | 0.030 |
| 48.75 | 0.39 | 0.0 | 5 | 0.00187 | 0.027 |
| 78.07 | 0.27 | 0.0 | 6 | 0.00130 | 0.019 |

PERCENT OF FUEL VAPORIZED
87.537

SAMPLING LOCATION B-1

| GAS VELOCITY AT PROBE TIP FT/SEC | CO2 % | CO PPM | UHC PPM | F/A RATIO | EQUIVALENCE RATIO |
|---|---|---|---|---|---|
| 267.79 | 0.23 | 0.0 | 11 | 0.00111 | 0.016 |
| 70.35 | 0.20 | 0.0 | 10 | 0.00096 | 0.014 |

Table 5

Spillover Tests - Gas Analysis

| Date | Time | Probe Location | Flow Meter Reading | Flow Meter Temperature (°F) | Flow Meter Pressure in. Hg | Gas Analysis $CO_2$ (%) | Gas Analysis CO (ppm) | Gas Analysis UHC (ppm) |
|---|---|---|---|---|---|---|---|---|
| 2/14/80 | 1216 | B-1 | 59 | 70 | +1.8 | 0.67 | 0 | 54 |
| | 1222 | B-1 | 45 | 70 | +1.2 | 0.51 | 0 | 30 |
| 2/15/80 | 1028 | B-3 | 58 | 70 | +1.7 | 6.85 | 6.0 | 14 |
| | 1030 | B-3 | 45 | 70 | +1.3 | 7.47 | 5.0 | 18 |
| | 1030 | B-3 | 30 | 70 | +0.6 | 8.55 | 3.0 | 0 |
| | 1040 | B-3 | 15 | 70 | -0.5 | 9.97 | 0 | 0 |
| | 1044 | B-4 | 55 | 70 | +1.4 | 5.65 | 0 | 12 |
| | 1047 | B-4 | 45 | 70 | +1.1 | 5.65 | 0 | 10 |
| | 1051 | B-4 | 30 | 70 | +0.6 | 7.02 | 0 | 6 |
| | 1055 | B-4 | 15 | 70 | -0.2 | 7.95 | 0 | 4 |
| | 1100 | B-4 | 50 | 70 | +1.3 | 5.22 | 0 | 5 |
| | 1105 | B-2 | 57 | 70 | +1.6 | 1.78 | 0 | 6 |
| | 1107 | B-2 | 42 | 70 | +1.2 | 1.78 | 0 | 4 |
| | 1110 | B-2 | 30 | 70 | +0.6 | 1.86 | 0 | 2 |
| | 1116 | B-2 | 15 | 70 | -0.5 | 2.24 | 0 | 12 |
| | 1121 | B-5 | 60 | 70 | +2.1 | 1.26 | 0 | 11 |
| | 1126 | B-5 | 45 | 70 | +1.5 | 1.26 | 0 | 8 |
| | 1129 | B-5 | 29 | 70 | +0.7 | 1.34 | 0 | 7 |
| | 1132 | B-5 | 15 | 70 | -0.7 | 1.57 | 0 | 5 |
| | 1136 | B-6 | 62 | 70 | +2.3 | 0.31 | 0 | 8 |
| | | B-6 | 30 | 70 | +0.8 | 0.43 | 0 | 5 |
| | | B-6 | 15 | 70 | -0.8 | 0.39 | 0 | 5 |
| | 1147 | B-6 | 45 | 70 | +1.8 | 0.27 | 0 | 6 |
| | 1200 | B-1 | 65 | 70 | +3.0 | 0.23 | 0 | 11 |
| | | | 20 | 70 | +0.3 | 0.20 | 0 | 10 |
| | 1527 | C-3 | 34 | 70 | +0.2 | 1.38 | 5 | 610 |
| | 1531 | C-3 | 15 | 70 | -3.3 | 1.22 | 5 | 12 |
| | 1535 | C-4 | 36 | 70 | +0.1 | 1.30 | 6 | 500 |
| | 1538 | C-4 | 15 | 70 | -3.0 | 1.34 | 5 | 10 |
| | 1605 | C-2 | 37 | 70 | +0.1 | 0.53 | 3 | 80 |
| | | C-2 | 15 | 70 | -3.2 | 0.39 | 3 | 10 |
| Recalibrated with 0-5% $CO_2$ | | | | | | | | |
| 2/15/80 | 1632 | C-5 | 39 | 70 | +0.2 | 0.26 | 0 | 150 |
| | | C-5 | 25 | 70 | +0.05 | 0.26 | 0 | 100 |
| | 1637 | C-5 | 15 | 70 | -2.9 | 0.24 | 0 | 10 |
| | 1646 | C-1 | 44 | 70 | +0.4 | 0.10 (too low) | 0 | 250 |
| | 1649 | C-6 | 42 | 70 | +0.3 | 0.10 | 0 | 120 |
| | 1708 | C-4 | 39 | 70 | +0.2 | 0.71 | 0 | 120 |
| | | C-4 | 25 | 70 | +0.1 | 0.70 | 0 | 100 |
| | 1715 | C-4 | 15 | 70 | -2.8 | 0.62 | 0 | 120 |
| | | C-3 | 41 | 70 | +0.2 | 0.80 | 0 | 120 |
| | | C-3 | 20 | 70 | 0.0 | 0.80 | 0 | 120 |

## Table 6

## Spillover Test Rig Data

| Date | Time | Temperature | | Orifice | | Rig | Fuel Flow | Catalytic Reactor Temperatures | | | |
|---|---|---|---|---|---|---|---|---|---|---|---|
| | | Orifice °F | Inlet °F | Press. PSIG | ΔP HG | Press. PSIG | CPS | Top | Mid | Bott. | Core |
| 2-14-80 | 11:15 | 680° | 720° | 65 | 11.8 | 59.5 | 136.7 | | | | |
| | 11:30 | 680° | 720° | 65 | 11.8 | 60.0 | 135.9 | | | | |
| | 11:45 | 680° | 720° | 65 | 12.1 | 59.0 | 135.9 | | | | |
| | 12:15 | 680° | 720° | 66 | 12.1 | 60.0 | 135.7 | | | | |
| 2-15-80 | 10:30 | 680° | 700° | 66 | 11.8 | 59.8 | 134.6 | 1903 | Out | 1183 | 700° |
| | 10:45 | 685° | 700° | 66 | 12.0 | 58.5 | 135.9 | 1751 | Out | 1207 | 792 |
| | 11:00 | 690° | 715° | 66 | 12.0 | 58.5 | 135.8 | 1056 | Out | 1304 | 845 |
| | 11:15 | 690° | 720° | 66 | 11.8 | 59.5 | 135.7 | 643 | Out | 1255 | 768 |
| | 11:30 | 690° | 720° | 66 | 11.8 | 59.5 | 135.2 | 475 | Out | 1309 | 665 |
| | 11:45 | 695° | 720° | 66 | 11.8 | 59.5 | 134.8 | 345 | Out | 1047 | 530 |
| | 3:15 | 695° | 725° | 66 | 11.8 | 60.0 | 128.6 | 553 | Out | 1170 | 826 |
| | 3:30 | 690° | 725° | 63 | 11.55 | 60.0 | 129.7 | 602 | Out | 1503 | 932 |
| | 4:30 | 690° | 725° | 66 | 11.8 | 59.9 | 129.8 | 513 | Out | 1279 | 761 |
| | 5:15 | 699° | 725° | 67 | 11.55 | 60.0 | 129.6 | 595 | Out | 1375 | 847 |

(2) Air Velocity: 16-point rectangular matrix

Series: AXAIR 1 - 30 cm plane
AXAIR 2 - 15 cm plane
AXAIR 3 - 7.5 cm plane

(3) Radial Air Velocity: 16-point matrix.

Series: RADAIR 1 - 39 cm plane
RADAIR 2 - 15 cm plane
RADAIR 3 - 7.5 cm plane

(4) Droplet Velocity/Size: 16-point matrix.

Series: SPRAY 1 - 30 cm plane
SPRAY 2 - 15 cm plane
SPRAY 3 - 7.5 cm plane

(5) Radial Droplet Velocity: 16-point matrix

Series: RADVEL 1 - 30 cm plane
RADVEL 2 - 15 cm plane
RADVEL 3 - 7.5 cm plane

# 4

# CONCLUSIONS

A new method of measuring fuel droplet size and velocity was developed during the mid 1970's. The significant factors in this method are the (1) simultaneous measurement of size and velocity and (2) the capability to measure the droplets in situ with no flow disturbing probes. The measuring instrument is based on the laser doppler velocimeter (LDV) principles.

While applications of this instrument can be found in many technical areas, the area of particular interest to gas turbine engines is the study of fuel sprays during fuel/air preparation and combustion in liquid fueled gas turbine engines. Once the fuel size and velocity characteristics are measured in an engine environment, combustion engineers will gain a more basic understanding of the fuel atomization process. The desired goal of this understanding is the production of low emission gas turbine combustors. The results could be applied to gas turbine combustors burning various types of heavy oils or synfuels.

Fuel spray characterization data was needed to calibrate and test an analytical model of lean premixed, prevaporized (LPP) combustors. To obtain data useful in the model development, a new measurement technique was developed.

In order to obtain the data, it was necessary to design and build a test rig with well-defined and controlled conditions. The rig was sucessfully completed and run for extended periods of time.

Optical measurements were successfully performed using a rig described above. The optical measurements included drop size and velocity distributions made at 30 points in three planes. The data were plotted and are consistent with expectations. This is the first known application of this technique to combustor fuel preparation investigations.

# APPENDIX A

## DETAILS OF SIZE DETERMINATION BY LDV
## METHODS OF LDV CALIBRATION

LDV MEASUREMENT CAPABILITIES

Spectron Development Laboratories (SDL) in close collaboration with John C. Meier of Solar, has developed an instrument for combustion research in gas turbine combustion system. The LDV instrument is unique in its capabilities of measurment of droplet size and two component velocities in the severe environment of an operating gas turbine combustor system. The instrument incorporates the following capabilities:

- Measurement of a two-dimensional velocity vector with a range of $\pm$(0.01-200 m/sec)
- Measurement of particle size when the particles are in the velocity range of 5-30 m
- Specification of probe volume position coordinates with a high degree of accuracy ($\pm$0.5 mm)
- Immediate on-line data checks
- Rapid computer storage of acquired data

The optical system of the LDV was constructed based on proven designs. The optial system is designed so the instrument can be used in the backscatter observation mode or 90 degrees off axis. The electronic system was built around an existing design which is capable of:

- Measuring signal visibility (proportional to particle size) for each velocity component
- Measuring signal time period (proportional to particle speed and velocity) for each velocity component
- Sorting data pertinent to particle size or velocity for each velocity component
- Producing the particle size and velocity data in a format compatible with digital computer recording systems

The optical system is mounted on a moveable platform which provides environmental protection and allows the oeprator to specify the position of the sample space with high accuracy. The system is designed for remote oepration. Table A-1 shows the general capabilities and system advantages.

Signal Analysis for Determination of Particle Size

A brief review of the basic principles which must be used to determine particle size from a measurement of signal shape in the LDV.

Table A-1

LDV General Description

1. The LDV determines particle size over a 10:1 size range via the relative magnitude of light scattered from particles passing through crossed laser beans interference fringes, and determines particle velocity over a $10^5$:1 range (not simultaneously)

2. The system is capable of measuring particle size, number density and velocity at a rate of 20,000 particles/sec for particles from 5 $\mu$m to 300 $\mu$m in diameter and $\pm$1 cm/sec to $\pm$200 m/sec.

3. Requires no material probes and therefore performs perturbation-less measurements.

4. Calibration for particle composition not required since size determination is not dependent on absolute measurement of radiation intensity.

5. High quality receiving optics not required.

6. With calibration LDV can be used to directly determine particle mass concentration.

Two equal-intensity, well-collimated, coherent light beams intersect at a common origin (geometric center) with an included angle, (Fig. A-1).

Huygen's diagram of the wavefronts shows that planar interference fringes are generated which are perpendicular to the plane defined by the beam centerlines and are parallel to the bisector between the beams. The distance between the periodic frings, $\delta$, is given by:

$$\delta = \lambda[2 \sin (\alpha/2)] \qquad (1)$$

where $\lambda$ is the wavelength of the coherent light. When a particle (assumed spherical) much less than $\delta$ in diameter crosses the fringe pattern, it can be assumed to be uniformly illuminated at all points along its path through the fringe pattern, and the light which is scattered by the particle is proportional to the observable flux illuminating it. Thus, measurement of the time period, $\tau$, of the scattered light is related to the velocity, v, of the particle through the relationship:

$$v = \delta/\tau \qquad (2)$$

As the size of the scattering particle increases relative to $\delta$, the illumination of the particle is no longer uniform and must be averaged over the cross-sectional area of the particle. The nonuniform illumination of the particle results in a reduction in the contrast or visibility of the scattered

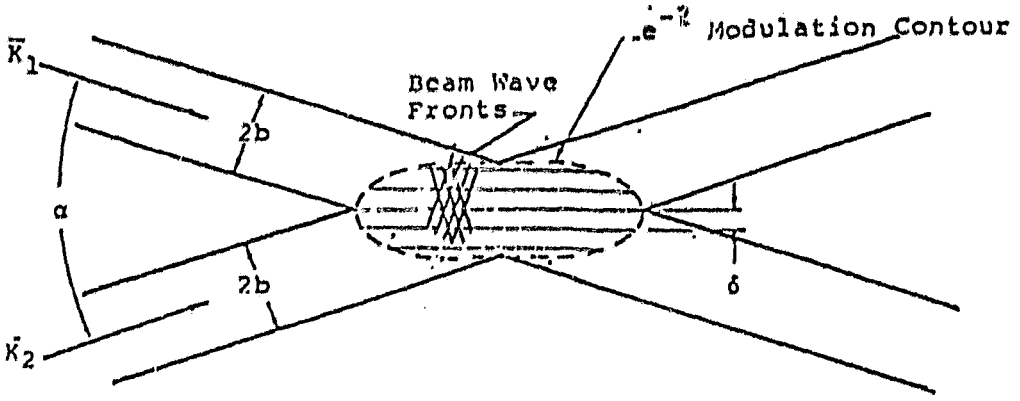


Figure A-1. Huygen's Diagram of Interference Fringe Generation in PM Probe Volume

light signal. Let $I_{max}$ by the maximum value in intensity in a period of the scattered light from a particle and $I_{min}$ the next successive minimum. The visibility, V, and then be defined as:

$$V = \frac{I_{max} - I_{min}}{I_{max} + I_{min}} \tag{3}$$

It is straightforward to show that V is fully equivalent to the ratio of AC amplitude divided by the DC amplitude of the scattered light signal. Henceforth, the high frequency "Doppler" portion of the signal will be referred to as the "AC". It usually has many cycles of information relative to that of the DC component, which refers to the Gaussian shaped low frequency terms describing the signal. Analytically, the visibility may be written as:

$$V \quad \frac{\int_{A_p} I_o \cos(2\pi t/\delta)\, dA_p}{\int_{A_p} I_o dA_p}$$

where $A_p$ is the cross-sectional area of the particle; $I_o$ is the intensity distribution across one of the illuminating beams; and y is the coordinate ormal to the fringe planes. When $I_o$ is a Gaussian function ($TEM_{00}$ laser beam), it can be shown that Equation (4) is an accurate approximation over a depth of field, $\ell$, given by:

$$\ell = 0.8\, b/\ , \tag{5}$$

where b is the radium of the $e^{-2}$ intensity point in the illumination beam. For depths of field greater than $\ell$, the signal visibility is a function of particle size and position in the illumination. To simplify Equation (4) for Guassian beams and still maintain accuracy, it is required that the particle diameter, D, satisfy the relationship:

$$D \leq 0.2\ b \tag{6}$$

and for $\delta$ to satisfy:

$$\delta \leq 0.2\ b \tag{7}$$

Under these conditions, V for a sphere can be written as:

$$V \simeq 2J_1\ (\pi D/\delta)/(\pi D/\delta), \tag{8}$$

where $J_1$ is a Bessel function of the first kind. For a cylinder, V can be written as

$$V \simeq \sin(\pi fL/\delta)/(\pi L/\delta). \tag{9}$$

Equations (8) and (9) are plotted in Figure A-2 to illustrate the salient features of the visibilty in particle size measurement.

Determination of particle size using a visibility measurement has a number of advantages over other optical techniques. Among the more important is the fact that:

- High quality, scattered-light-collecting systems are not required.
- A visibility measurement can determine particle size to, at least, 10 times better than the resolution limit of the transmitting lens.
- True particle flux rate, i.e., mass concentration, may be determined with the LDV system.
- Size measurements may be made from backscattered light.

On the other hand, disadvantages in using this technique are also apparent. For example, application of the LDV system must account for the fact that:

- Size measurement is particle shape dependent.
- High quality, transmitting optical systems are required.
- Particle size measurement of spheres is limited to approximately a 15:1 size variation range for a given fringe period.
- High quality spatially coherent light is required for good interference fringe quality.
- The particle size measuring ability is limited by the frequency response of the signal process in electronics.

The last item results from the fact that the signal frequency is velocity dependent. Hence, an instrument which measures signal visibilty is limited to the measurement of particle with velocities which are less than those which produce a signal frequency greater than the frequency response limit of the instrument.

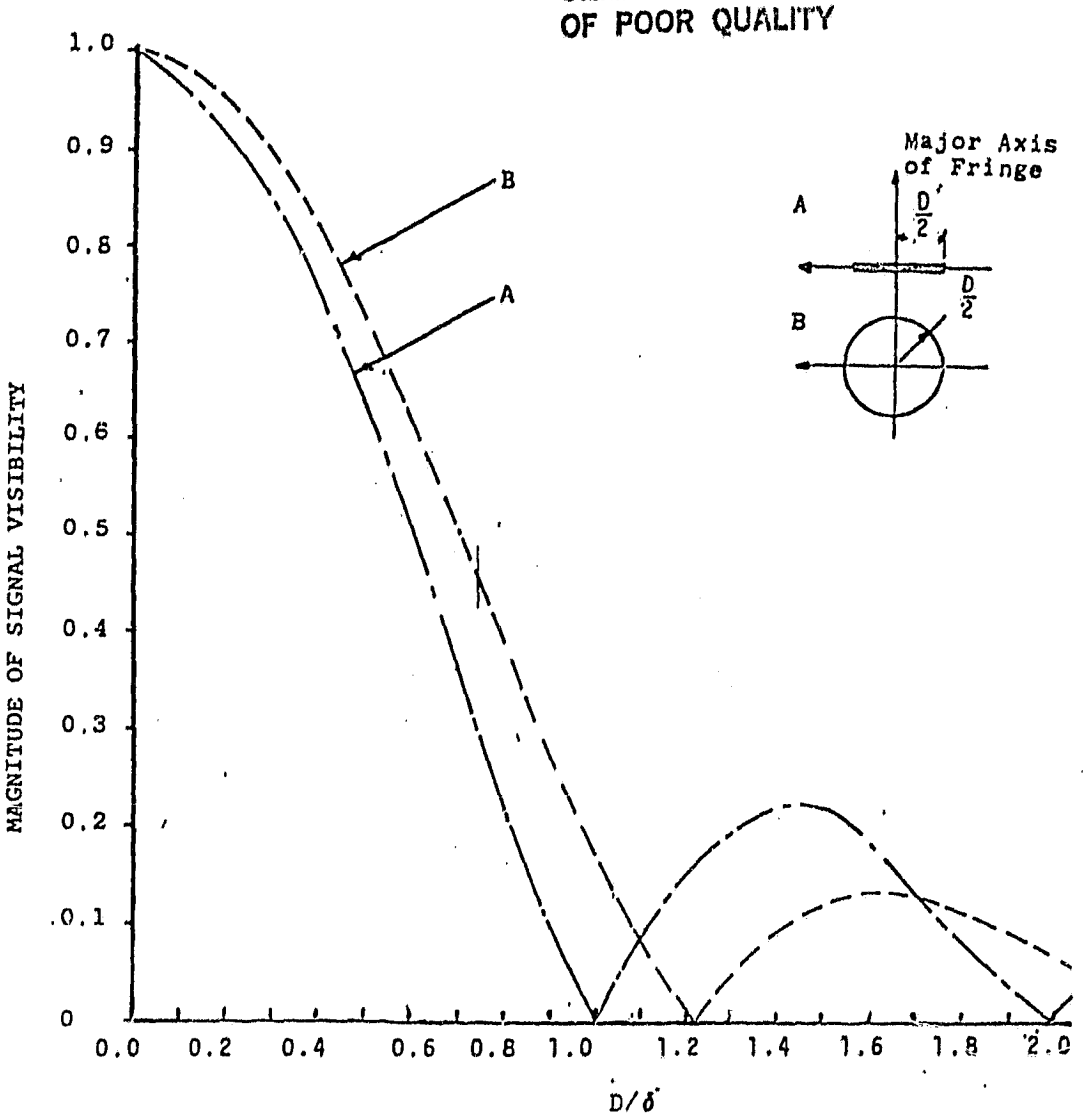


Figure A-2. Visibility as a Function of $D/\delta$ for Two Particle Shapes

A summary of the principles of operation of the LDV is provided in Table A-2. A schematic representation and interpretation is summarized in Tables A-3 and A-4.

## Signal Processing Considerations

To minimize error in the estimate of particle size, it is of utmost importance that signal visibility be measured with high accuracy and precision. This is due to the fact that signal visibility error and particle size error are not linearly related. For spherical particles, Figure A-3 illustrates the particle diameter uncertainty for several different values of visibility. As the figures show, where the ratio of particle diameter D to fringe period $\delta$ is near 1, the particle diameter uncertainty is the same as the visibility un-

Table A-2

Principle of LDV Operation

| |
|---|
| 1. Two equal intensity, coherent light beams are mixed at an angle. |
| 2. A well-defined set of equally spaced interference fringes is formed by interference of the two beams. |
| 3. Light scattered by a particle traversing the fringe set is modulated according to size and position of the particle. |
| 4. Particle size is determined from the ratio of the amplitudes of (1) the modulated scattered intensity to (2) the average scattered intensity. |
| 5. Particle velocity is determined by measurement of the signal time period. |

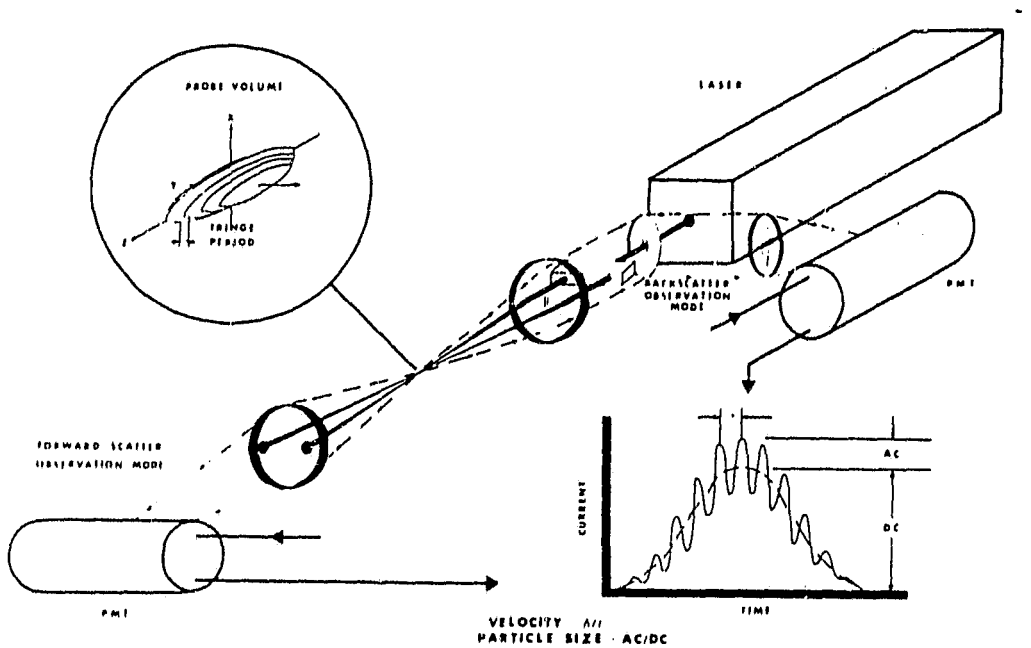


Figure A-3. Interferometric Measurement of Velocity and Particle Size

Table A-3

Signal Description

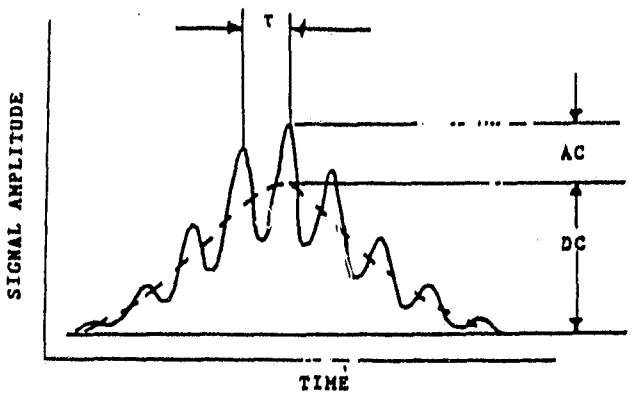


1. The signal contains two components in amplitude
   - the modulated scattered intensity of ac component
   - the average scattered intensity of dc component
2. The time period, $\tau$, of the modulated scattered intensity is a function of particle velocity.

Table A-4

Signal Parameters and Particle Characteristics

1. Particle velocity v is computed from

   $$v = \delta/\tau$$

2. Particle size is computed from signal visibility

   $$\upsilon = ac/dc$$

3. For spherical particles of diameter D

   $$\upsilon = 2J_1(\pi D/\delta)/(\pi D/\delta)$$

   $J_1(\ )$ is a first order Bessel function of first kind

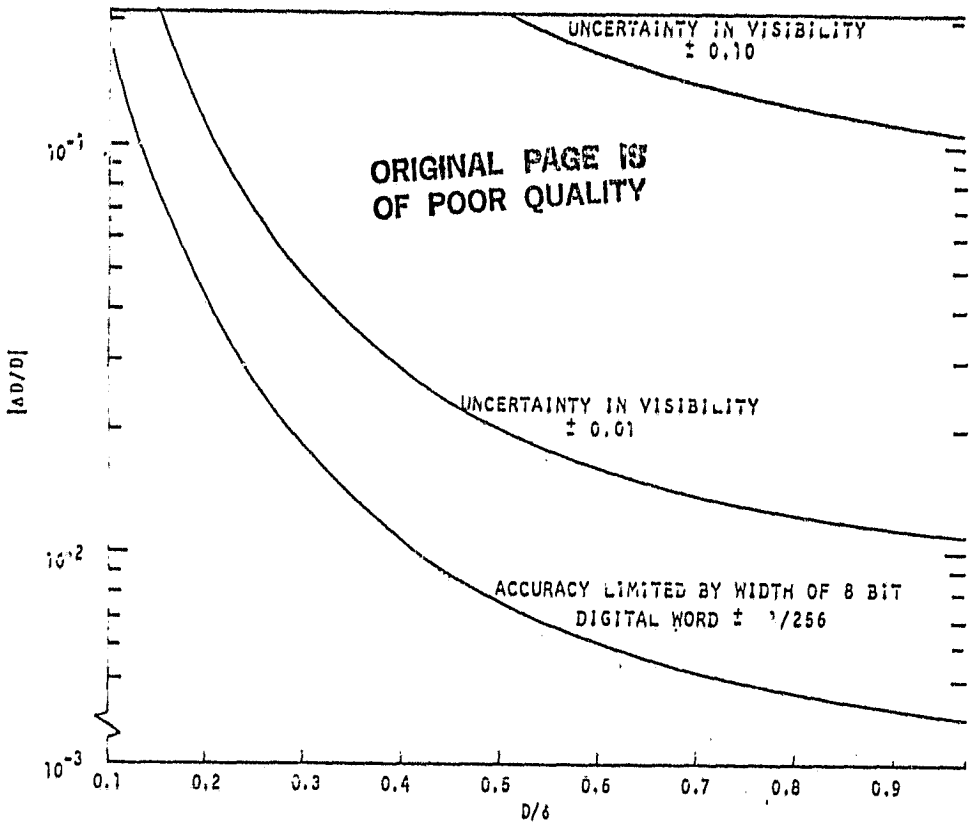


Figure A-4. Uncertainty in Spherical Particle Diameters for Various Values of Uncertainty in the Visibility

certainty is the same as the visibility uncertainty. However, as $D/\delta$ decreases, particle diameter uncertainty rapidly increases. Thus, when $D/\delta$ is small, the error in particle size will be much greater than that in the visibility. An instrument which measures signal visibility must seek to minimize errors in the visibilty measurements if an accurate particle size measurement is to be obtained.

Potential Sources of Error in a Signal Visibility Measurement

In examining the LDV signal, a number of potential error sources are evident which could produce considerable error in a visibilty measurement. Among the most important error sources are:

- Signal noise
- Asymmetric signal shapes
- Variations in the signal visibility
- Signals resulting from more than one particle.

Signal noise may result from any number of sources but is usually either broad band, Gaussian-distributed noise occurring during the entire duration of the signal; single, very-high-frequency spikes which occur randomly in the signal; or periodic amplitude variations which mix with the signal. The first two forms of noise are usually evident when signal magnitudes are low. The third form usually results from a radiative pickup from high-power consuming or generating instruments operating across the entire frequency spectrum. Asymmetric signal shapes result form particles with trajectories that do not pass through the optical axis of the probe volume. Such signals can also arise through turbulence induced distortions in the signal (Fig. A-5). Variations in signal visibilty occur when $D/\delta$ is near 1, and the AC component of the signal has only a few cycles of information relative to that of the DC component. Signals resulting from more than one particle usually generate aperiodic signals of skewed shapes. The LDV optical designs account for the possibility of multiple particle signals by generating a probe volume which is small enough to produce a low probability of observing more than one particle. Certain types of error logic may also be used in the signal processing electronics to reject such signals.

Visibility From Signal Integration. To minimize the errors which may result from "real world" LDV signals, it is most desirable to observe and measure as much of the signal as possible. One method of satisfying this requirement is through integration of the entire signal (within preset limits). Consider a particle whose trajectory passes through or near the geometric center of the probe volume. It can be shown that the visibility obtained by computing the integral of the DC component, and the integral of the full-wave rectified value of the AC component, and by dividing the integrated DC into the integrated AC is (to within a known numerical factor) identical to that measured for a single cycle measured at the center of the signal. Integration of the signal is most desirable because the noise components previously listed will contribue very little to an integral value of the signal. For example, Gaussian-distributed white noise and periodic noise have zero or nearly zero values for an integration, and high-frequency-noise spikes contribute very little to the overall integral value. Furthermore, integration of asymmetric signals tends to reduce the effects of the asymmetry by producing an overall signal average. The primary difficulty in using a signal integration to determine the signal visibility resides in the fact that the dynamic response of an integrator will be affected by large frequency variations in the signal input. Thus, without design precautions, an integator could produce considerable error in attempting to measure particle size in turbulent flows where there are considerable velocity variations.

Signal Amplitude Constraints. While a visibilty measurement is independent of signal magnitude, detailed considerations must be given to relative signal amplitude in order for a visibility measuring instrument to have a sufficient dynamic range in amplitude response.

For particles of identical index of refraction and of a size greater than about 5 $\mu$m, i.e., for particles with scattering gain coefficients independent of particle size, the signal amplitude can be expected to vary by a factor of 100 over the measurable size range. Probable volume intensity variations can

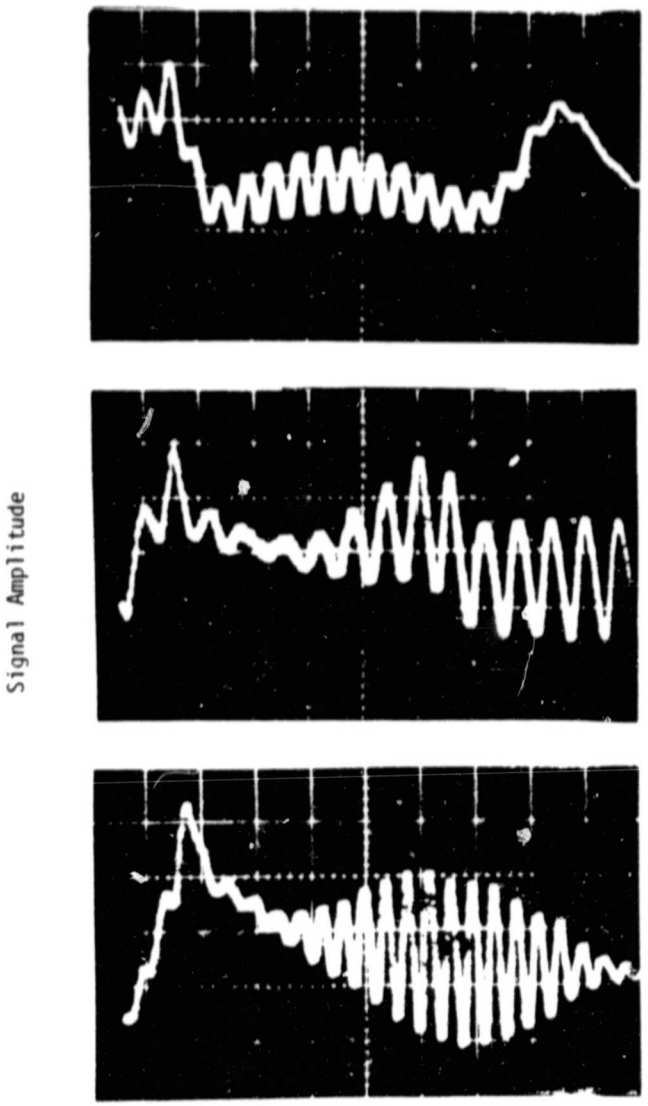


Figure A-5. Example of LDC Signal Distortions Resulting From Flame Turbulence

be expected to range over facrors of 10 in each of two orthogonal probe volume dimensions. Thus, an instrument must be capable of responding to relative signal amplitude variations of at least $10^3$:1 and, more reasonably, $10^4$:1. Linear amplifiers can cover a linear dynamic range of approximately $10^2$ for a single-range setting. The designer is thus faced with the difficulty of producing an instrument which at one range setting can cover sufficient dynamic range to eliminate instrumental bias in particle size measurements.

One technique to overcome the dynamic range limitation is the use of logarithmic amplifiers. For example, if an integration technique is used to determine

the signal visibilty from a logarithmically amplified signal, it can be shown that the visibility is given by:

$$V = \text{sech}[\int \ell n(i_{AC}) - \int \ell n(i_{DC})], \quad (10)$$

where $\int \ell n(i_{AC})$ is the integrated logarithmically amplified AC component of the signal and $\int \ell n i_{DC})$ is the integrated DC component. Logarithmic amplifiers can easily cover a dynamic range of $10_4$:1 for low frequency signals, making an instrument much more sensitive to small particle signals. The primary difficulty with such amplifiers is that their sensitifity is a strong function of signal frequency and quickly decreases as the frequency increases, making their effectiveness questionable at the carrier frequencies involved with the laser flame analyzer.

Another solution to this limitation is obtained in using the integration approach to visibility measurement. An integrator can be designed to cover a 10:1 dynamic range visibility processor designed by SDL personnel utilizes four parallel integration circuits each overlapping the other in range so that for a given signal frequency a dynamic amplitude range of $10^4$:1 with three-digit accuracy can be covered. Such accuracy gives an acceptable error in particle size determined by a visibility measurement even when the particle size is small.

## LDV CALIBRATIONS

The LDV is a recently developed instrument and as such requires attention to the methodology of calibration. Four separate experimental procedures were developed to achieve a high confidence level in the calibration and therefore in the data from the instrument. The experiments are the monodispersed droplet generator, the spinning disc velocity calibrator, the nitrogen tunnel for simultaneous particle size and velocity measurements and comparison with data from a calibrated spray nozzle. (A second method would be used to calibrate the spray nozzle.)

### Monodispersed Droplet Generator

A droplet generator was successfully designed, built and tested on non-program funds. The generator produces a stream of liquid droplets (water) of uniform diameter in the range 20-300 microns. A built-in deflection circuit allows the experimenter to divert one droplet (minimum diameter 40 micron) at regular intervals. The diversion of a single droplet is critical to calibration since the LDV probe volume can only contain that one droplet without signal dropout. Optical verification techniques (photomicrographs) of the same drop being measured by the LDV will give the LDV user confidence in the size data. A photograph of the stream of droplets produced by the Solar monidispersed generator is in Figure A-6. The deflection of one droplet can be seen in that photo.

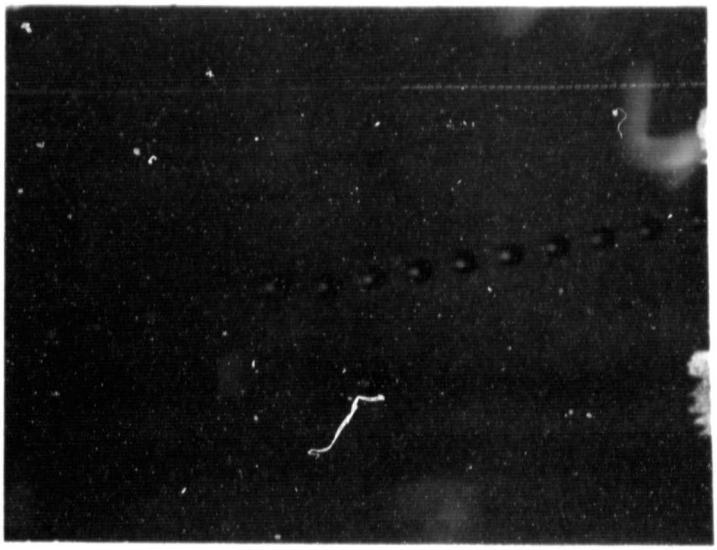

Figure A-6. Monodispersed Droplet Stream (100 Microns)

An overall view of the equipment used to make the droplets is shown in Figure A-7. Basically, the droplets are formed by the passage of the liquid through a vibrating orifice plate. Pulsed deflection plates downstream of the orifice deflect the chosen droplet if the liquid has been lightly doped with an electrolyte. The entire droplet generating head is mounted on the XYZ micro-positioning translator.

Spinning Disc

The spinning disc calibration consists of a motor driven disc with one wire protruding radially from its circumference. The circumference of the wheel is known. The rotational speed of the wheel is accurately measured by a frequency counter. Thus the wire passes through the probe volume at a precisely known translational velocity. Velocities can be controlled up to 100 m/s. The equipment is pictured in Figure A-8. A scope trace taken after the passage of the wire through probe volume is shown in Figure A-9. The characteristic LDV signal trace is seen there.

The LDV was successfully calibrated for velocity accuracy using this technique. The calibrations were performed for four fringe periods at one transmitter focus, 40 inches, and one scan distance, 20 inches. Two channels of the LDV were calibrated at the four fringe periods and the entire calibration was performed a second time in reverse order to check for systematic errors. At each fringe period, the instrument was checked at six different velocities. Five separate sets of one hundred measurements were made at each velocity. In total, 48,000 measurements were made during the fringe period (velocity) calibration. The data from the fringe period calibration exists on several pages. A typical data sheet is reproduced in Figure A-10. A statistical analyses of that data is shown near the bottom of that figure.

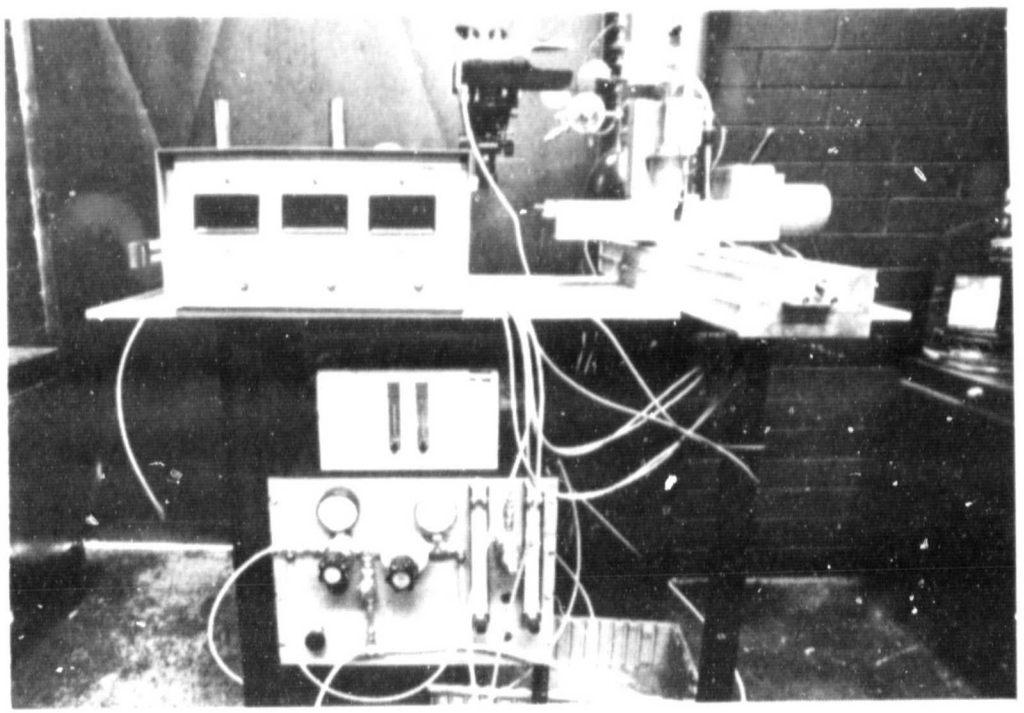

Figure A-7. Monodispersed Droplet Generator Mounted on XYZ Positioner

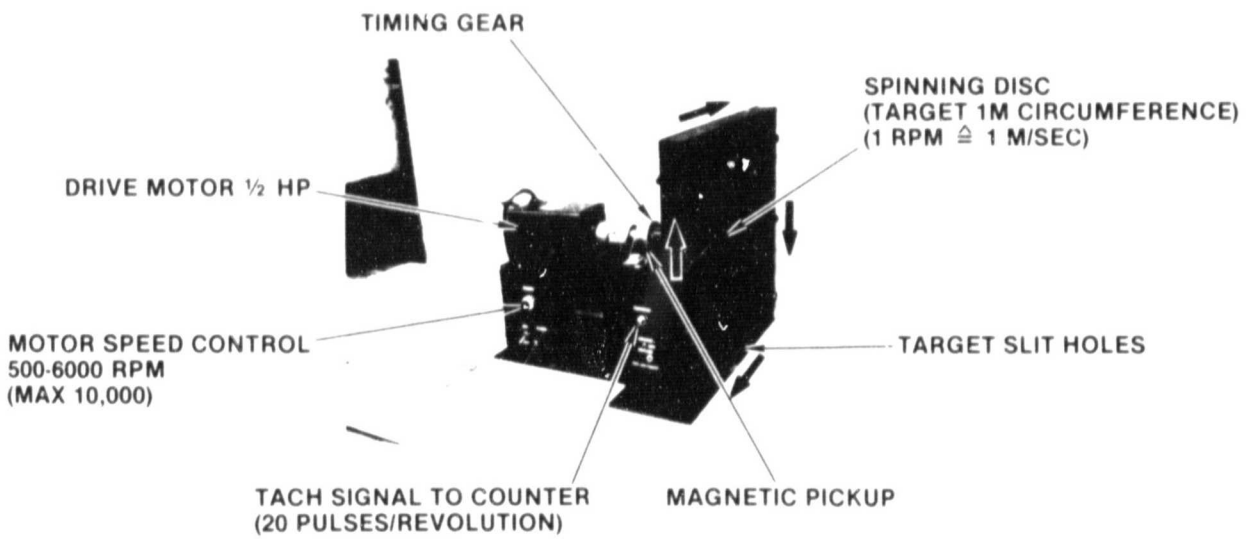


Figure A-8. LDV Spinning Disc With Target for Velocity Calibration

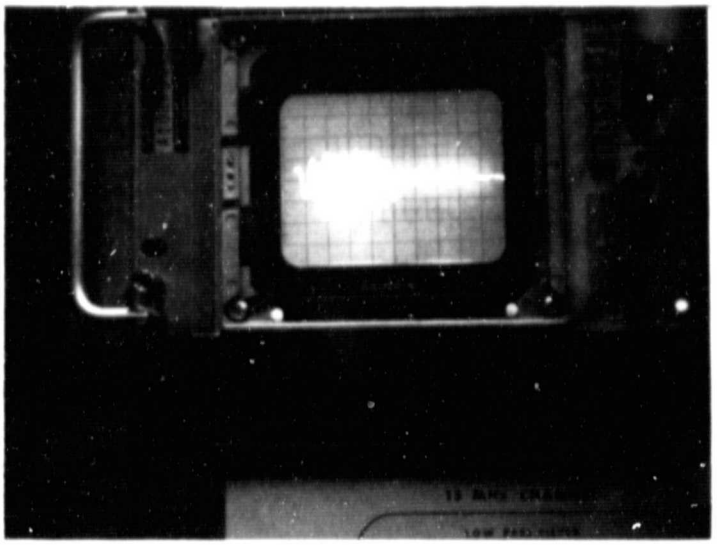

Figure A-9. Scope of Trace of LDV Signal

A summary of all data points is shown in Figure A-11. The standard deviations are less than one percent and most are less than 0.5 percent of the fringe period.

Nitrogen Tunnel

The nitrogen tunnel experiment was designed, built, calibrated and tested on non-program funds (Solar). The purpose of this device is to calibrate the LDV for size and velocity simultaneously. Particles or beads of a known size are injected into an airstream of known and controlled velocity. The LDV measures the size and velocity of the group of particle as they exit the tunnel. A catch basin is provided to remove the spent particles from the atmosphere. The gas used is pure, high pressure nitrogen, boiled from an $LN_2$ supply. That uniform gas enters the test tunnel from the top (see Fig. A-12), passes through flow straighteners, and encounters a throttle. Gas pressure and temperature are measured just above the throttle. Three throttle plates were built. Each was calibrated in the tunnel by the Colorado Experimental Station in Boulder, Colorado. The gas passing the plate enters a venturi section in which the particles are injected. To insure uniform distribution of the particles in the air stream, they are fed from a fluidized bed into six ports placed symmetrically around the tunnel just above the venturi. For small particles the six injectors are perpendicular to the gas stream. For heavier particles a second set of injectors pointing 15 degrees upstream is used. The calibrator is totally operational.

| Run Number | 1<br>Disc Frequency (counts) | 2<br>Calculated Disc Velocity (1 ÷ 20) (m/s) | 3<br>$V_{measured}$ | 4<br>Calculated Fringe Period (2 ÷ 3) (μ) |
|---|---|---|---|---|
| 1 | 172 | 8.60 | 12.17 | 70.67 |
| 2 | 172 | 8.60 | 12.16 | 70.72 |
| 3 | 171 | 8.55 | 12.13 | 70.49 |
| 4 | 171 | 8.55 | 12.10 | 70.66 |
| 5 | 171 | 8.55 | 12.15 | 70.37 |
| 6 | 403 | 20.15 | 28.71 | 70.18 |
| 7 | 404 | 20.20 | 28.62 | 70.58 |
| 8 | 412 | 20.60 | 29.17 | 70.62 |
| 9 | 417 | 20.85 | 29.67 | 70.27 |
| 10 | 428 | 21.40 | 30.49 | 70.19 |
| • | | | | |
| • | | | | |
| • | | | | |
| 26 | 1210 | 60.50 | 82.99 | 72.90 |
| 27 | 1207 | 60.35 | 84.34 | 71.56 |
| 28 | 1209 | 60.45 | 85.22 | 70.93 |
| 29 | 1208 | 60.40 | 82.81 | 72.94 |
| 30 | 1210 | 60.50 | 84.00 | 72.02 |

$$V_{measured} = \frac{\lambda}{\tau} = \frac{1}{\tau} = f_{measured}$$

$$\lambda = \frac{V_{calibration}}{f_{measured}} = \frac{V_{calibration}}{V_{measured}}$$

STATISTICAL ANALYSIS

Number of data points $n = 30$ runs of 100 replications each
Mean fringe period $\bar{x} = 70.78 \quad 68.59 \leq x_i \leq 72.92$
Standard deviation $s_x = 0.73 \quad \pm 3_\sigma = \pm 2.19$
Standard deviation of mean $\sigma_{\bar{x}} = 0.13$
True value of $x = 70.78 \pm 0.13$

OPERATING PARAMETERS

| Lens Number | Setting |
|---|---|
| L-2 | 0.96 |
| L-3 | 685 |
| L-4 | 3070 |
| L-5 | 6.0 |
| Transmit | 60.11 |
| Receiver | 3.420 |
| Power | 750 mV |
| PMT | 300 V |
| Line # | 7 |

Figure A-10. Typical Fringe Period Calibration Data Sheet

| Channel A Fringe Period Horizontal Velocity Compression | Standard Deviation | Channel B Fringe Period Vertical Velocity Compression | Standard Deviation |
|---|---|---|---|
| 82 | 0.1 | 56 | 0.6 |
| 105 | 0.4 | 70 | 0.3 |
| 160 | 0.4 | 105 | 0.1 |
| 278 | 1.4 | 179 | 0.4 |

Figure A-11. Summary of Fringe Period Calibration Data

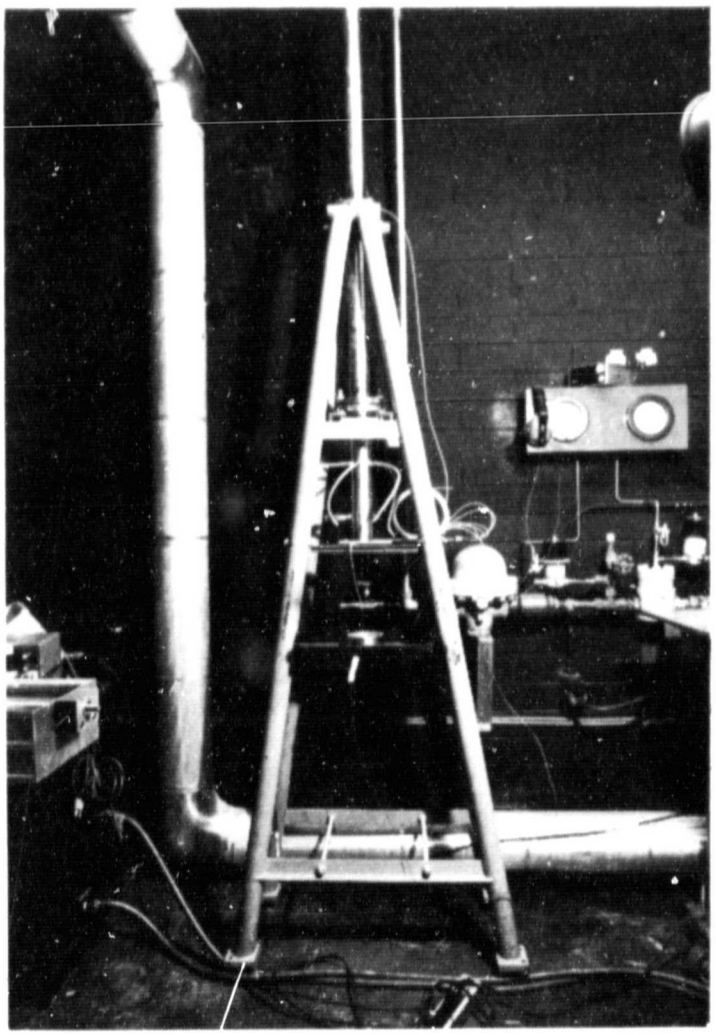

Figure A-12.

Nitrogen Tunnel Experiment

## Calibrated Spray Nozzle

The intent of this experiment is to measure the droplet size and velocity distributions from a pressure atomizing spray nozzle calibrated by another method and compare the data from the two methods. This was not accomplished during the period of the reported effort.

# APPENDIX B

# VAPORIZATION COMPUTER CODE

```
1000 REM CALCUALTION OF DEGREE OF VAPORIZATION
1010 REM NASA-SOLAR LASER RIG
1020 REM SPILLOVER TECHNIQUE
1030 DIM R$[2,5],V$[2,5],C$[2,5],M$[2,5],H$[2,5],A$[8],B$[8]
1031 DIM B$[5,5],N$[5,5],C$[8]
1032 PRINT TAB21"NASA-LEWIS/SOLAR LASER RIG"
1033 PRINT TAB14"VAPORIZATION DATA VIA SPILLOVER TECHNIQUE"
1034 DISP TAB5"INPUT DATE AND FUEL";
1035 INPUT A$,B$
1036 PRINT
1037 PRINT TAB22"DATE:"A$,TAB40"FUEL: "B$
1038 PRINT
1040 DISP TAB8"INPUT RIG DATA";
1050 INPUT T1,T2,P1,D1,P2,C1
1060 REM RIG DATA IS AS FOLLOWS
1070 REM T1=ORIFICE TEMP,DEG F
1080 REM P1=ORIFICE PRESS, PSIG
1090 REM D1=ORIFICE PRESS. DROP, IN HG
1100 REM T2=RIG TEMP,DEG F
1110 REM P2=RIG PRESS., PSIG
1120 REM C1=CYCLES/SEC FUEL FLOW
1130 REM CALCULATION OF AIR DENSITY AT ORIFICE == R1
1140 R1=2.7023*(P1+14.7)/(T1+460)
1150 REM CALCULATION OF AIR FLOW RATE, ===  R2
1160 R2=4606.09*SQR(R1*D1)
1170 REM CALC OF FUEL FLOW RATE == F1
1180 F1=0.991*C1+4
1190 REM CALC OF ISOKINETIC VELOCITY IN RIG == V0
1200 REM CALC OF AIR DENSITY AT RIG CONDITIONS==R3
1210 R3=2.7023*(P2+14.7)/(T2+460)
1220 V0=0.003264*R2/R3
1221 REM CALC OF RIG FUEL/AIR RATIO
1222 R0=F1/R2
1230 PRINT TAB9"ORIFICE      ORIFICE     ORIFICE     RIG        RIG"
1240 PRINT TAB10"TEMP         PRESS      DELTA P     TEMP     PRESS"
1250 PRINT TAB11"F           PSIG       IN HG       F          PSIG"
1260 FORMAT 9X,F4.0,10X,F5.1,6X,F5.1,6X,F4.0,6X,F5.1
1270 WRITE (15,1260)T1,P1,D1,T2,P2
1280 PRINT
1290 PRINT
1300 PRINT TAB9"FUEL FLOW     AIR FLOW      FUEL/AIR         MEAN ISOKINETIC"
1310 PRINT TAB9"LB/HR         LB/HR         RATIO            VELOCITY, FT/SEC"
1320 FORMAT 9X,F6.1,8X,F7.1,6X,F8.5,14X,F6.1
1330 WRITE (15,1320)F1,R2,R0,V0
1334 PRINT
1340 REM INPUT DATA FOR EACH SAMPLING POINT
1350 DISP "INPUT NO. OF PTS AND LOCATION";
1360 INPUT P,C$
1364 PRINT
1365 PRINT TAB4"SAMPLING"
1366 PRINT TAB4"LOCATION"
```

```
1367 PRINT TAB5,C$
1370 DISP "INPUT ROTAMETER AND GAS ANLAYSIS DATA";
1380 FOR J=1 TO P
1390 INPUT M[1,J],H[1,J],B[1,J],B[4,J],B[5,J]
1391 REM M(1,J)= ROTAMETER READING , DIVISIONS  605 TUBE , SS FLOAT
1392 REM H(1,J)= ROTAMETER PRESSURE, IN HG
1400 NEXT J
1402 GOSUB 4000
1403 GOSUB 5000
1405 GOSUB 7001
1412 GOSUB 6000
1413 DISP "NEW RIG DATA 1(YES) 0(NO)";
1414 INPUT A
1415 IF A=1 THEN 1040
1416 GOTO 1350
1453 END
3999 STOP
4000 REM SUBROUTINE FOR CALC OF FUEL/AIR RATIOS
4010 REM B(1,J)= PERCENT CO2
4020 REM B(4,J)= PPM CO
4030 REM B(5,J)= PPM UHC
4040 REM A8= FUEL RATIO H/C
4041 A8=1.9
4050 REM N(1,J)= F/A RATIO EMISSIONS
4060 REM N(2,J)= EQUIVALENCE RATIO EMISSIONS
4070 S1=34.3719636-274.219526/(12.01+A8)
4080 FOR J=1 TO P
4090 N1=(0.0001*(B[4,J]-B[1,J]*0.68)+B[1,J])*(1+A8/2*10↑(-6)*B[5,J])
4100 N2=100+A8/4*B[1,J]+(0.0001*(B[4,J]-B[1,J]*0.68)*(A8/4-0.5))
4110 N[1,J]=N1*(12.01+A8)/28.89/N2
4111 R[1,J]=N[1,J]
4120 N[2,J]=N[1,J]*S1
4121 NEXT J
4141 RETURN
4150 END
4999 STOP
5000 REM SUBROUTINE FOR CALC OF V(1,J) SAMPLING VEL AT PROBE TIP
5010 FOR J=1 TO P
5020 REM FIRST CALC SAMPLING RATE SCFM AT STP= C(1,J)
5030 C[1,J]=(0.2903*M[1,J]-0.871)*SQR((29.92+H[1,J])/29.92)*0.0005885
5040 V[1,J]=C[1,J]*1515.62*(T2+460)/(P2+14.7)
5041 NEXT J
5060 RETURN
5070 END
5999 STOP
6000 REM SUBROUTINE FOR CALC OF DEGREE OF VAPORIZATION
6010 REM BASED ON LEAST SQUARES FIT OF DATA
6020 W1=0
6030 X1=0
6040 Y1=0
6050 Z1=0
6060 FOR J=1 TO P
```

```
6070 W1=W1+(V0/VL1,JJ)^2
6080 X1=X1+(V0/V[1,JJ)
6090 Y1=Y1+(R[1,JJ/R0)
6100 Z1=Z1+(V0/V[1,JJ)*(R[1,JJ/R0)
6110 NEXT J
6120 REM SOLVE OF DEGREE OF VAP
6130 B=(Z1-(Y1*W1)/X1)/(X1-(P*W1)/X1)
6140 M=(Y1-B*P)/X1
6141 E=B/(B+M)*100
6142 PRINT
6151 PRINT TAB24"PERCENT OF FUEL VAPORIZED"
6152 FORMAT 30X,F8.3
6153 WRITE (15,6152)E
6160 RETURN
6170 END
7000 STOP
7001 REM SUBROUTINE FOR DATA  PRINTING
7120 PRINT
7122 PRINT TAB5"GAS VELOCITY"
7123 PRINT TAB5"AT PROBE TIP    CO2      CO       UHC        F/A  EQUIVALENCE"
7124 PRINT TAB8"FT/SEC          %       PPM      PPM       RATIO    RATIO"
7133 FOR J=1 TO P
7134 FORMAT 7X,F7.2,6X,F5.2,2X,F5.1,2X,F6.0,4X,F8.5,6X,F6.3
7135 WRITE (15,7134)V[1,J],B[1,J],B[4,J],B[5,J],N[1,J],N[2,J]
7140 NEXT J
7141 RETURN
7143 END
```